

Chapter 1

Fast Pulsars, Neutron Stars, and Astrophysical Strange Quark Matter Objects

Delaney Farrell

*Department of Physics, San Diego State University
5500 Campanile Drive, San Diego, CA 92182, USA
Email: dfarrell@sdsu.edu*

Fridolin Weber

*Department of Physics, San Diego State University
5500 Campanile Drive, San Diego, CA 92182, USA
Department of Physics, University of California at San Diego
9500 Gilman Drive, La Jolla, CA 92093, USA
Email: fweber@sdsu.edu, fweber@ucsd.edu*

Milva G. Orsaria*, Ignacio F. Ranea-Sandoval**, Martín Canullán§

*Grupo de Astrofísica de Remanentes Compactos
Facultad de Ciencias Astronómicas y Geofísicas
Universidad Nacional de La Plata
Paseo del Bosque S/N, La Plata (1900), Argentina
Consejo Nacional de Investigaciones Científicas y Técnicas (CONICET)
Godoy Cruz 2290, Buenos Aires (1425), Argentina
Email: *morsaria@fcaglp.unlp.edu.ar, **iranea@fcaglp.unlp.edu.ar,
§canullanmartin@fcaglp.unlp.edu.ar*

Rodrigo Negreiros

*Catholic Institute of Technology
1 Broadway - 14th floor, Cambridge, MA 02142
Instituto de Física, Universidade Federal Fluminense, Niterói, Rio de Janeiro,
Brazil
Email: rnegreiros@id.uff.br*

Takashi Katayama†, Ian Wagaman‡

*Department of Physics, San Diego State University
5500 Campanile Drive, San Diego, CA 92182, USA
Email: †tkatayama0396@sdsu.edu, ‡iwagaman6967@sdsu.edu*

Abstract: This book chapter explores key aspects of neutron stars, pulsar glitches, tidal deformability, fast pulsars, the equation of state, and strange quark matter stars. Challenges in directly measuring neutron star radius have led to reliance on spectroscopic and timing techniques, with uncertainties addressed through careful source selection and theoretical modeling. Pulsar glitches reveal insights into the equation of state through angular momentum transfer within the neutron star. Tidal deformability is crucial in gravitational-wave astronomy, exemplified by the GW170817 event. Fast pulsars, instrumental in astrophysical testing, are classified into ordinary pulsars, millisecond pulsars, and magnetars. The EOS is vital for understanding neutron star internal structure, explored through various models. The chapter delves into the theoretical framework for rotating neutron stars, addressing uniform and differential rotation scenarios and their impacts on mass and radius. Additionally, the intriguing concept of quark stars and strange dwarfs is investigated. The various topics discussed in this book chapter contribute to a broader understanding of dense matter physics, astrophysical phenomena, and the potential for transformative discoveries through advanced observational techniques and technologies like gravitational wave detectors, radio telescopes, and X-ray telescopes.

Keywords: Neutron stars; Quark stars, Pulsars, Nuclear equation of state; Strange quark matter, Stellar rotation

Contents

1. Title	1
<i>Delaney Farrell</i>	
<i>Fridolin Weber</i>	
<i>Milva G. Orsaria*</i> , <i>Ignacio F. Ranea-Sandoval**</i> , <i>Martín Canullán[§]</i>	
<i>Rodrigo Negreiros</i>	
<i>Takashi Katayama[†]</i> , <i>Ian Wagaman[‡]</i>	
1.1 Introduction	4
1.2 Observation	6
1.2.1 Observed Neutron Star Properties	6
1.2.2 Fast Pulsars	11
1.3 Equation of State	13
1.3.1 Nuclear Matter	13
1.3.2 Strange Quark Stars and Strange Quark Matter	17
1.4 Properties of Strange Dwarfs	22
1.5 Properties of Rotating Neutron Stars	24
1.5.1 Uniform Rotation	25
1.5.2 Differential Rotation	29
1.6 Summary and Concluding Remarks	34
<i>Bibliography</i>	39

1.1 Introduction

Neutron stars stand out as the densest observed stellar objects, typically harboring masses within the range of 1 to 2 solar masses (M_{\odot}) and radii spanning from 10 to 15 km. The immense gravitational forces at play within neutron stars compress the matter in their innermost regions to densities exceeding nuclear saturation density (2.5×10^{14} g/cm³), turning neutron stars into inherent laboratories for investigating ultra-dense matter [Alford (2001); Haensel *et al.* (2007); Alford *et al.* (2008); Becker (2009); Blaschke and Chamel (2018); Sedrakian *et al.* (2023)]. Notably, neutron star matter is one of the densest forms of matter in the Universe and also exists in its ground state, characterized by temperatures that are less than 10^{10} K (or around 1 MeV), effectively registering as zero temperature on the nuclear scale. The cold, superdense matter encapsulated within neutron stars occupies a unique temperature and density regime that cannot be replicated in terrestrial laboratories, such as the Relativistic Heavy-Ion Collider or the Large Hadron Collider (ATLAS-Collaboration *et al.*, 2008), which are only capable of probing superdense matter in the high-temperature domain. Despite decades of theoretical, experimental, and observational endeavors, understanding the properties of cold, superdense matter remains a forefront area of nuclear and astrophysics.

Determining the equation of state (EOS), which defines the relationship between pressure, density, and temperature of neutron star matter, holds paramount importance [Özel and Freire (2016); Sedrakian (2007); Lattimer and Prakash (2016); Burgio *et al.* (2021); Sedrakian *et al.* (2023)]. This endeavor not only aids in unraveling the nature and characteristics of the strong interaction but also enhances our comprehension of various astrophysical phenomena, including core-collapse supernovae, binary neutron star mergers, and the early Universe.

In addition to the intrinsic significance of neutron stars, a multitude of factors contribute to the evolving landscape of neutron star research. Pulsars, characterized by their intense and precisely timed radiation, offer unique insights into the dynamics of these enigmatic objects. Moreover, the advent of new observational data facilitated by powerful telescopes has significantly advanced our understanding of neutron stars (Kaspi and Gavriil, 2017). Notably, the (1) FAST (Five hundred meter Aperture Spherical Telescope) stands out as a remarkable instrument capable of detecting extremely faint radio signals from space (Nan *et al.*, 2016). This capability has rapidly expanded the number of pulsar observations, providing invaluable insights into the behavior of neutron stars. In addition to FAST, several other state-of-the-art observatories and instruments lead the forefront of neutron star research. Positioned on the International Space Station, (2) NICER (Neutron star Interior Composition Explorer): NICER serves as an X-ray telescope meticulously designed to scrutinize the interior composition of neutron stars, delving into the intricacies of their dense cores (Gendreau *et al.*, 2016). (3) eROSITA (Extended Roentgen Survey with an Imaging Telescope Array): Functioning as an X-ray instrument on the Spektrum-Roentgen-Gamma mission, eROSITA conducts a comprehensive survey of the X-ray sky (Predehl *et al.*, 2021). Its capabilities significantly contribute to the exploration of neutron stars and other high-energy astrophysical phenom-

ena. (4) Chandra X-ray Observatory: This space telescope, specifically engineered for observing X-rays emanating from high-energy regions of the universe proves invaluable in the study of neutron stars (Weisskopf *et al.*, 2000). (5) XMM-Newton: Serving as an X-ray observatory designed for high-resolution X-ray spectroscopy, XMM-Newton has played a pivotal role in advancing our understanding of neutron stars and their surrounding environments [Jansen *et al.* (2001)]. (6) VERITAS (Very Energetic Radiation Imaging Telescope Array System): Contributing to the study of neutron stars emitting high-energy gamma rays, VERITAS enhances our exploration of these celestial objects (Holder *et al.*, 2006). (7) LOFAR (Low-Frequency Array): A vast radio telescope array spanning Europe, LOFAR offers unique capabilities for low-frequency radio observations, providing a valuable avenue for studying pulsars and other radio-emitting neutron star phenomena (van Haarlem *et al.*, 2013). (8) Green Bank Observatory: Instrumental in the examination of pulsars and other radio-emitting neutron star phenomena, the Green Bank Observatory plays a significant role in advancing our understanding of these cosmic entities (Hughes *et al.*, 2006). (9) Jodrell Bank Observatory: The observatory's radio telescopes, including the Lovell Telescope, have been instrumental in observing and monitoring pulsars, aiding in the understanding of these highly magnetized, rotating neutron stars. The precise timing of pulsar signals is crucial for research, including the search for gravitational waves (Jodrell Bank Observatory, Accessed: January 2022). Last but certainly not least, (9) the Parkes telescope is a state-of-the-art facility for radio astronomy, distinguishing itself in the study of neutron stars and pulsars (Johnston *et al.*, 1996). Collectively, these observatories and instruments represent a comprehensive and cutting-edge approach to unraveling the mysteries of neutron stars.

Beyond conventional neutron stars, the intriguing possibility of strange quark stars, composed of strange quark matter, adds an extra layer of complexity to our exploration. Strange quark matter is a speculative and exotic form of matter theorized to exist at exceedingly high densities. According to the hypothesis surrounding strange quark matter, it is envisioned as a composition of up, down, and strange quarks – the fundamental particles constituting protons, neutrons, and hyperons. The proposition suggests that strange quark matter may possess greater stability than conventional nuclear matter, with quarks moving freely rather than being confined within protons and neutrons. Should such matter indeed exist, it could give rise to new categories of compact stellar objects, ranging from compact strange stars, with bulk properties akin to massive neutron stars, to strange quark matter dwarfs, representing the strange counterparts of ordinary white dwarfs. Despite the elusive nature of experimental verification for the existence of strange quark matter, its theoretical implications are pivotal in advancing our understanding of astrophysical phenomena and the fundamental building blocks of matter under ultra-high-density conditions.

In this chapter, we delve into the intricate theoretical modeling of neutron stars, compact strange stars, and strange dwarfs, placing particular emphasis on the influence of rapid stellar rotation. Our investigation encompasses the examination of

both differential and rigid body rotation. The primary objective is to comprehensively explore the properties inherent in these stellar objects and discern the pivotal role played by strange quark matter in interpreting the nature of compact stellar entities.

1.2 Observation

Observation of neutron stars has been perhaps the most important catalyst to furthering our knowledge on the subject since their theorized existence. In the last two decades, there has been an increasing amount of high-quality, new data from X-ray and gamma-ray telescopes, including precisely timed observations of pulsars (Özel and Freire, 2016). Today, over 3,000 pulsars have been discovered, and their discoveries have provided valuable constraints on various neutron star properties like mass and radius, cooling (Slane *et al.*, 2002), and magnetic fields (Makishima *et al.*, 1999). Additionally, these measurements provide constraints on the cold EOS of superdense matter (Lattimer and Prakash, 2007; Dietrich *et al.*, 2020), a long-standing mystery in nuclear astrophysics. As we move into an era of new-generation X-ray telescopes, these constraints on neutron star properties and EOS are expected to tighten even further; these discoveries will also aid in our understanding of other astrophysical phenomena like core-collapse supernova, r-process nucleosynthesis, and gravitational wave emission (Özel and Freire, 2016).

1.2.1 Observed Neutron Star Properties

1.2.1.1 Mass

The mass of neutron stars is perhaps the most precisely measured neutron star property, especially those coming from radio pulsar timing of neutron star masses in compact binaries (Watts *et al.*, 2016). Observed values of masses of neutron stars (Lattimer, 2016) are extremely valuable measurements as they test theories of nuclear matter and therefore provide constraints on the nuclear EOS. A notable example of such a constraint resulted from the observation of massive neutron stars. For several decades the canonical mass of a neutron star was $1.4 M_{\odot}$, but recent observations of heavier neutron stars ($\geq 2 M_{\odot}$) have widened the range of masses that must be accounted for with theoretical EOS models. Heavy neutron stars directly challenge theoretical models of dense nuclear matter in quantum chromodynamics (QCD). Observations of massive stars enforced the requirement that EOS models for neutron star matter must produce maximum stable masses of at least $2 M_{\odot}$. Such models are referred to as "stiff" meaning they have a large pressure for a given density, so observations of massive neutron stars ruled out many softer theoretical EOS models. An example of such massive observations is MSP J0740+6620 with a measured mass of $2.14^{+0.10}_{-0.09} M_{\odot}$, making it one of the heaviest millisecond pulsars observed thus far (Cromartie *et al.*, 2020).

Radio pulsars, or highly magnetized, rotating neutron stars, that exist in binary stellar systems generate radio pulses that can be precisely tracked as a method of determining the binary's mass (Özel and Freire, 2016). Radio pulsars have long-

term rotational stability, allowing for very precise timing measurements of orbital motion. The binary mass function, $f(M_1, M_2, i)$, can be derived from measurements of five Keplerian parameters: the binary period P_b , the projection of the pulsar's orbital semimajor axis a on the line of sight $x \equiv a_i \sin i$, the orbital eccentricity e , and time T_0 and longitude ω_0 of periastron ω (Weber, 1999). The formula for the mass function is given as

$$f(M_1, M_2, i) \equiv \frac{(M_2 \sin i)^3}{(M_1 + M_2)^2} = \frac{P_b v_1^3}{2\pi G} = \frac{4\pi^2 x^3}{GP_b^2}, \quad (1.1)$$

where G is Newton's gravitational constant and $v_1 = (2\pi/P_b)x$ is the orbital velocity of star M_1 along the line of sight. Other relativistic effects, like the transverse Doppler effect and gravitational redshift, can also be used to determine the pulsar and companion's masses in a binary system (Özel and Freire, 2016; Weber, 1999).

Alongside other parameters, mass can also be inferred from stellar emission using other observational techniques like waveform modeling, where a Bayesian inference approach is employed to analyze X-ray waveform oscillations emitted by pulsars (Miller and Lamb, 2015; Miller *et al.*, 2019). X-ray oscillations can be observed from accretion-powered pulsars, thermal emission of rotation-powered (or non-accreting) pulsars, or some thermonuclear bursts on accreting neutron stars (Watts *et al.*, 2016). It is believed that the X-ray oscillations are emitted from a "hot spot" on the star's surface, or a region of the stellar surface that is both hotter than its surroundings and offset from the rotational pole of the star. The pulse profile, or waveform, from the hot spot combined with general relativistic effects like light bending and Doppler boosting, can be used to determine the mass and radius of the source. Pulse waveform modeling was pioneered using data from X-ray telescopes like ROSAT and XMM-Newton, but the methodology has become more popular recently with observations from NICER, which has extraordinary absolute timing accuracy when determining the pulse profile of isolated neutron stars and those in binary systems (Miller *et al.*, 2019). For example, NICER data was used to determine estimations for the mass and radius of the isolated millisecond pulsars PSR J0030+0451 (Riley *et al.*, 2019; Miller *et al.*, 2019) and PSR J0740+6620 (together with XMM-Newton data) (Riley *et al.*, 2021; Miller *et al.*, 2021). The latter study showed that although having a mass $\sim 40\%$ larger, the radii of PSR J0740+6620 and PSR J0030+0451 are of the same order (Riley *et al.*, 2019; Miller *et al.*, 2021). This finding is all the more interesting when considering that the determination of neutron star radius has historically been more difficult than mass, which is discussed further below.

1.2.1.2 Radius

Historically, direct measurements of neutron star radius do not exist, and inference of radius using various techniques provides large uncertainties when compared to precise mass measurements. Current methods for determining radius commonly rely on the spectroscopic measurements of surface emission to either measure apparent angular size or look for effects of the emission on neutron star spacetime (Özel

and Freire, 2016; Watts *et al.*, 2016). These methods broadly fall into one of two categories: spectroscopic or timing measurements.

Spectroscopic measurements from either the surface emission of quiescent low-mass X-ray binary (LMXB) systems or from thermonuclear bursts can be used to constrain the mass-radius relation. If it is assumed that the surface spectrum is a diluted blackbody and the source of the spectrum is at a known distance D , the mass-radius (M-R) relation of a slowly spinning neutron star can be defined as

$$R^2 \left(1 - \frac{2GM}{Rc^2} \right)^{-1} = \frac{FD^2 f_c^4}{\sigma T_c^4}, \quad (1.2)$$

where F is the measured flux, σ is the Stefan-Boltzmann constant, and T_c and f_c are the color temperature and color-correction factor, respectively (Watts *et al.*, 2016). The color temperature is assumed to be larger than the star's effective temperature, defined as $T_c = f_c T_{\text{eff}}$. The color-correction factor f_c is dependent on both the assumed atmospheric composition and effective surface gravity, where $f_c \approx 1.3 - 2$ (Watts *et al.*, 2016). Under the same assumed conditions, the observed or apparent radius R_{obs} can be defined as

$$R_{\text{obs}} = R \left(1 - \frac{2GM}{Rc^2} \right)^{-1/2}. \quad (1.3)$$

The above approximation is reliant on several assumptions and exact measurements and thus may not hold in various instances. In the case of strong magnetic fields, for example, the assumptions of a specific atmospheric composition and a constant surface temperature may be incorrect (Özel and Freire, 2016). For rotating neutron stars that are rotating rapidly (i.e. not spinning slowly), spin-dependent corrections must be applied to the observed angular size as the spacetime can not be described by a Schwarzschild metric due to frame dragging (Özel and Freire, 2016). Additional complications to the approximation are introduced if there is uncertainty when measuring the exact distance D to the star.

Some uncertainties can be alleviated by choosing sources with low magnetic fields or those that exist in globular clusters of known distances, which is why thermal emission from sources like low-mass X-ray binaries (LMXBs) in quiescence are at the forefront of constraining the neutron star mass-radius relation. The observed thermal spectrum can be fit to a well-motivated theoretical model dependent on the assumed atmosphere of the neutron star in a process called spectral fitting. Many of these theoretical models assume quiescent LMXBs have pure hydrogen atmospheres as the companion stars are hydrogen-rich, but other atmospheric compositions like helium and carbon have also been explored in the literature (Steiner *et al.*, 2018).

As mentioned in the section above, the mass-radius relation can also be explored through X-ray timing techniques like waveform modeling, spin measurements, and asteroseismology. While further explanation of these techniques will not be discussed explicitly, the reader can find more information at Miller *et al.* (2019); Sotani *et al.* (2011); Watts *et al.* (2016); Miller *et al.* (2021).

1.2.1.3 Pulsar Glitches and Moment of Inertia

A pulsar “glitch”, or sudden spin jump, is another observable property that can help constrain our knowledge of the EOS of dense neutron star matter. Rotation-powered pulsars will generally experience a slow and gradual spin down from the emission of magnetic dipole radiation, leading to very regular rotational periods (Piekarewicz *et al.*, 2014). However, some pulsars will experience abrupt spin-ups, leading to a deviation from their otherwise regular rotational periods.

The mechanism driving these glitches is an angular momentum transfer between the star’s solid outer crust and a portion of the liquid interior (Link *et al.*, 1999). A popular model to explain the angular momentum transfer relies on the theory that a pulsar will form vortex lines in the neutron superfluid formed within the inner crust (at densities of 10^{11} to 10^{14} g/cm³). A rapidly rotating pulsar can have superfluid vortices with extremely high areal densities, and the spin up or spin down of the superfluid is dependent on increasing or decreasing the vortex density (Alpar *et al.*, 1984; Piekarewicz *et al.*, 2014). The superfluid velocity is thus determined by the spatial arrangement of vortex lines (Weber, 1999). If the vortex lines were assumed to be pinned to a crystal lattice of neutron-rich nuclei, the angular velocity of the superfluid would be largely fixed and appear to be rotating as a rigid body (Piekarewicz *et al.*, 2014). The pulsar will slow down by the emission of magnetic dipole radiation, and as the crust’s angular velocity slows down from magnetic torque, the difference between the velocity of the crust and the superfluid regime grows. When this differential rotation between the slower crust and faster superfluid vortices grows too large, some vortex lines become unpinned and suddenly transfer angular momentum to the crust - resulting in a glitch (Weber, 1999).

To date, 671 glitches from 224 pulsars have been recorded using high-precision pulsar timing (an extensive and well-maintained list can be found in the Jodrell bank glitch catalog (Basu *et al.*, 2022)). While most pulsars have glitches infrequently and irregularly, others like the Vela or Crab pulsar have quasi-periodic glitches (Piekarewicz *et al.*, 2014). An extremely unique case is PSR J0537-6910, the fastest spinning young pulsar recorded, which exhibits large glitches roughly every 100 days (Abbott *et al.*, 2021).

The magnitude of a pulsar glitch is dependent on the star’s moment of inertia I , another global neutron star property. A pulsar glitch of magnitude $\Delta\Omega_i$ requires the angular momentum

$$\Delta J_i = I_c \Delta\Omega_i \quad (1.4)$$

where I_c is the moment of inertia of both the star’s crust and coupled interior core, estimated to make up 90% or more of the star’s total moment of inertia (Link *et al.*, 1999). Between each glitch, the rotating interior acts as an angular momentum reservoir at a rate of \dot{J}_{res} . This rate is constrained by the average spin-down rate of the crust $\dot{\Omega}$ and the moment of inertia of the reservoir I_{res} as (Link *et al.*, 1999)

$$\dot{J}_{\text{res}} \leq I_{\text{res}} |\dot{\Omega}|. \quad (1.5)$$

The ratio of the moment of inertia of the reservoir I_{res} and the moment of inertia

of the crust I_c provides the lower limit of

$$\frac{I_{\text{res}}}{I_c} \geq \frac{\Omega}{|\dot{\Omega}|} A = G \quad (1.6)$$

where A is the pulsar's glitch activity parameter and G is the coupling parameter that describes the minimum fraction of I that stores and imparts angular momentum to the crust in the glitch (Link *et al.*, 1999; Piekarewicz *et al.*, 2014). The moment of inertia can be expressed in terms of mass and radius, so constraining the upper and lower limits can therefore also provide valuable constraints on the dense matter EOS.

1.2.1.4 Tidal Deformability and Gravitational Waves

The tidal deformability of compact objects is an important physical quantity for gravitational-wave astronomy. The main reason is that it determines the pre-merger GW signal in binary neutron star merger events. Working up to linear order, the tidal deformability λ is given by

$$\lambda = -\frac{\varepsilon_{ij}}{Q_{ij}}, \quad (1.7)$$

where ε_{ij} denotes the external gravitation field produced by the external source and Q_{ij} is the induced mass-quadrupolar moment of the given object. In addition, λ is related to the second Love number, k_2 , and the radius of the compact object, R , by

$$\lambda = \frac{2}{3} k_2 R^5. \quad (1.8)$$

Finally, the dimensionless tidal deformability, Λ , is defined by

$$\Lambda = \frac{\lambda}{M^5}, \quad (1.9)$$

where the M denotes the gravitational mass of the compact star. For details on how theoretical calculations related to this quantity are performed, the interested reader can refer to Refs. Hinderer (2008); Han and Steiner (2019) and references therein.

The detection by LIGO and Virgo observatories of the gravitational waves emitted during event GW170817, a binary neutron star merger (see, for example, (Abbott *et al.*, 2018) and references therein) together with its electromagnetic counterpart (see, for example, [Abbott *et al.* (2017)], and references therein) allow to estimate the possible masses, radius and dimensionless tidal deformability of the merging objects. Additionally, the dimensionless tidal deformability of a canonical neutron star was estimated to be $\Lambda_{1.4} = 190^{+390}_{-120}$ at a 90% level with no strong restrictions to the EOS are imposed (Abbott *et al.*, 2018).

1.2.2 *Fast Pulsars*

Pulsars were first discovered in 1967 by Jocelyn Bell Burnell and Antony Hewish, who detected radio-wave pulses with rapid regularity from an unknown source (Hewish *et al.*, 1979). Just one year later, Thomas Gold proposed that pulsars are rapidly rotating, highly magnetized neutron stars that emit radio waves from their magnetic poles. Since their discovery, pulsars have served as valuable resources for testing theories of relativistic astrophysics and as a tool for the discovery of astrophysical phenomena like the existence of dark matter (De Luca *et al.*, 2021) or the gravitational wave background (Agazie *et al.*, 2023). To date, there have been over 3,000 pulsars observed, and this number will continue to grow as new radio, X-ray, and gamma-ray telescopes are constructed.

Pulsars can broadly be classified into three categories: ordinary pulsars, millisecond pulsars (MSPs), and magnetars. Ordinary or normal pulsars have rotational periods P between 0.1 to 3 s and magnetic fields of roughly 10^{12} G. This class of pulsars will spin rapidly early in their lifetime ($\lesssim 10^4$ years) but slow as they age, eventually disappearing from view (Melrose, 2017). MSPs, also referred to as recycled pulsars, are old neutron stars that have been recycled (spun up) by the accretion of mass and angular momentum from a low-mass companion (Manchester, 2017). MSPs have spin periods on the order of 1.4 to 20 ms and smaller magnetic fields ($B < 10^{11}$ G) when compared to the other two classes of pulsars. The last class, magnetars, are slowly rotating pulsars with extremely high magnetic fields (10^{14} - 10^{15} G). The radio emission from all three types of pulsars generally tends to fall into a relatively narrow frequency range of ~ 100 MHz to 10 GHz, with a smaller subset of pulsars producing high-energy emission. The three categories of pulsars can be differentiated with two measured parameters: the pulse period P and its rate of change \dot{P} , which can be used to determine other important quantities like the star's rotational frequency, spin-down rate, luminosity, characteristic age, and braking index (Melrose, 2017).

As shown by Glendenning *et al.* (1997), a potential signal of quark deconfinement in the core of a pulsar could be the alteration in the timing structure of a pulsar's spin-down. Should quark deconfinement transpire within their cores, the moment of inertia could decrease significantly as the matter in the core undergoes deconfinement to quark matter. This reduction in the moment of inertia leads to an acceleration in rotation, causing an abrupt change in the pulsar's spin-down rate. This transition is identifiable through the examination of the braking index which would differ drastically from its canonical value of ~ 3 . Calculations suggest that the braking index may even approach infinity as quark deconfinement is initiated in the stellar core.

As mentioned previously, measuring the stable rotation of pulsars provides valuable constraints on observable properties. The most precise timing measurements come from MSPs, which commonly exist in binary systems with low-density companions like white dwarfs. The small number of isolated MSPs are believed to have lost their companion in some way. For low-mass binaries, this could be from disruptions resulting from the pulsar's strong relativistic winds; for higher-mass double

neutron star systems, the orbit could be disrupted by the supernova explosion of the secondary star (Lorimer, 2008).

The fastest pulsar observed thus far is PSR J1748–2446ad, discovered first in 2004 and confirmed in 2005 (Hessels *et al.*, 2006). This radio pulsar is located in the globular cluster Terzan 5, which has the largest known population of globular cluster MSPs. PSR J1748–2446ad spins at an impressive frequency of 716 Hz, with a pulse period P of 1.39595482 ms, and a pulse derivative \dot{P} of $\leq 6 \times 10^{-19}$ (Hessels *et al.*, 2006). Before the discovery of PSR J1748–2446ad, the fastest MSP detected was the first MSP ever detected, PSR 1937+21, spinning at a frequency of 642 Hz (Rawley *et al.*, 1987). A table of various MSPs with spin periods of ≤ 2 ms can be found in Table 1.1.

Table 1.1: Sample millisecond pulsars (MSPs) with rotational periods P of $\lesssim 2$ ms not associated with a globular cluster. Included are the rotational periods P , year discovered, and the telescope used in the observation (PKS: Parkes Radio Telescope, GBT: Green Bank Telescope, GMRT: Giant Metre Wave Radio Telescope, MK: MeerKat, FAST: Five Hundred Meter Aperture Spherical Radio Telescope). Table adapted from (Lorimer and Ferrara, 2022).

PSR Name	P (ms)	Year	Telescope
J0034-0534	1.88	1994	PKS
J0955-6150	1.99	2013	PKS
J1023+0038	1.69	2009	GBT
J1036-4353	1.68	2021	MK
J1221-0633	1.93	2017	GBT
J1227-4853	1.69	2014	GMRT
J1301+0833	1.84	2010	GBT
J1555-2908	1.79	2017	GBT
J1723-2837	1.86	2012	PKS
J1747-4036	1.65	2009	PKS
J1804-2858	1.49	2018	PKS
J1810+1744	1.66	2009	GBT
J1831-6503	1.85	2022	MK
J1833-3840	1.87	2015	PKS
J1843-1113	1.85	2004	PKS
J1849+0016	1.81	2020	FAST
J1859+0313	1.61	2019	FAST
J1902-5105	1.74	2009	PKS
J1924+2027	1.95	2020	FAST
J2036-02	1.91	2020	GBT
J2051+50	1.68	2020	GBT

1.3 Equation of State

The essential physics of matter within a neutron star can be succinctly summarized by the EOS, which describes the pressure-density relation within the star. As discussed earlier in the chapter, the matter within the core of a neutron star exists in a low-temperature, high-density regime that cannot be replicated in laboratories or particle colliders. Instead, the EOS of dense neutron star matter must be described by theoretical models that vary widely due to particle composition and mathematical frameworks used. In this section, we discuss the physics of neutron star matter and explore the theoretical implication of the inclusion of quark matter on the EOS.

1.3.1 Nuclear Matter

The density of matter within a neutron star varies greatly from the crust to the core, ranging from a few grams per cubic centimeter at the surface to around 10^{15} g/cm³ at the core. The lower density regime spans from the star's surface to its outer and inner crust regions, while the higher density regime comprises the star's core region. As stated in the Introduction, the density within the innermost part of the core region may experience densities exceeding nuclear saturation density (2.5×10^{14} g/cm³), giving rise to more exotic types of matter like meson condensates, deconfined quark matter, and strange matter - all of which alter the matter's EOS.

The least dense portions of a neutron star are its surface and outer crust region, where matter is compressed to densities up to 10^6 g/cm³. The surface region is comprised of ordinary atomic nuclei (such as ⁵⁶Fe) and non-relativistic electrons and emits the thermal radiation observed by the telescopes discussed in Section 1.2. In the outer crust, at densities of $7 \times 10^6 - 4.3 \times 10^{11}$ g/cm³, electrons become relativistic and form a relativistic electron gas. Additionally, the atomic nuclei grow more neutron-rich while forming a solid Coulomb lattice. The final portion of the lower-density regime is the inner crust, existing at densities of $4.3 \times 10^6 - 2 \times 10^{14}$ g/cm³. In the inner crust, atomic nuclei grow extremely neutron-rich to the point neutrons begin to drip out of the nuclei and populate free states; the neutron-rich heavy metals form clusters in a solid lattice and are then immersed in a gas of relativistic electrons and neutrons (Lorenz *et al.*, 1993; Pethick *et al.*, 1995; Pethick and Ravenhall, 1999; R uster *et al.*, 2006; Chamel and Haensel, 2008).

The high-density region of a neutron star, its core, is composed of a relativistic Fermi liquid of neutrons and protons in the conventional description. The liquid is extremely neutron-rich while maintaining a certain fraction of protons, electrons, and muons to maintain chemical or β -equilibrium. The condition for β -equilibrium is given as

$$\mu_B = \mu_n + q_B(\mu_e - \mu_{\nu_e}), \quad (1.10)$$

where μ_B is the chemical potential of baryons B , neutrons (μ_n), electrons (μ_e), and electron neutrinos (μ_{ν_e}), while q_B is the baryon electric charge. The dense, neutron-rich matter in the core may reach densities of up to 10 times nuclear saturation density, and as nucleons at such high densities begin to overlap, the matter

is expected to transition into non-nucleonic states of matter. These states can take several forms: the onset of quark degrees of freedom and deconfined quark matter (Ivanenko and Kurdgelaidze, 1965; Itoh, 1970a; Collins and Perry, 1975; Fritzsche *et al.*, 1973; Baym and Chin, 1976; Keister and Kisslinger, 1976; Chapline and Nauenberg, 1977b,a; Fechner and Joss, 1978), boson condensates formed by pions or kaons (Migdal, 1972; Sawyer and Scalapino, 1973; Brown and Weise, 1976; Haensel and Proszynski, 1982; Mannarelli, 2019; Kaplan and Nelson, 1988; Nelson and Kaplan, 1987; Brown *et al.*, 1994; Lee *et al.*, 1994; Knorren *et al.*, 1995; Schaffner and Mishustin, 1996; Glendenning and Schaffner-Bielich, 1999; Malik *et al.*, 2021; Thapa *et al.*, 2021), or the formation of other matter with a high degree of strangeness. Due to the weak interactions in the cold and dense neutron star core, strange states of matter can form hyperons (Ambartsumyan and Saakyan, 1960, 1961; Leung and Wang, 1971; Pandharipande, 1971; Moszkowski, 1974; Bethe and Johnson, 1974) or color superconducting phases (Rajagopal and Wilczek, 2001; Alford, 2001; Rischke, 2004; Alford *et al.*, 2008). Additionally, the existence of self-bound compact stars consisting of strange quark matter has also been discussed in the literature and will be further explained in the next section (Witten, 1984; Terazawa, 1979; Alcock *et al.*, 1986a; Alcock and Olinto, 1988; Terazawa, 1991; Madsen, 1999; Weber, 2005; Madsen, 2007).

While the matter within the core of a neutron star cannot be replicated in terrestrial laboratories, properties of laboratory neutron-rich nuclei can be used to define the EOS for the crust (up to order 10^{11} g/cm³). The crust regions are thin, contributing very little to the bulk properties of the star like its mass and radius. Today, two commonly used EOS models for the crust include Baym-Pethick-Sutherland (Baym *et al.*, 1971b) and Baym-Bethe-Pethick (Baym *et al.*, 1971a) (BPS-BBP), or Harrison-Wheler (Harrison *et al.*, 1965) and Negele-Vautherin (Negele and Vautherin, 1973) (HW-NV).

For matter within the core, various theoretical approaches that can broadly be broken into two categories, phenomenological and *ab initio*, are employed to describe the dense, asymmetric many-body system. Phenomenological models, or relativistic mean-field (RMF) models, are constructed to reproduce properties of finite nuclei and nuclear matter (Tong *et al.*, 2018). For in-depth discussions concerning constraints on the equation of state of high-density matter extracted from nuclear physics and astrophysics, we refer to Lattimer and Steiner (2014); Lattimer (2019); Stone (2021).

Ab initio methods instead start with realistic free-space nucleon-nucleon (NN) interactions applied to the nuclear many-body system (Sammarruca, 2008). NN interactions, based on scattering data from free nucleons and properties of the deuteron, are characterized by a repulsive core at short distances, a strong attraction in an intermediate range, and are dominated by the one-pion exchange at large distances (Machleidt *et al.*, 1987; Machleidt, 1989). *Ab initio* methods of this kind include the quantum Monte Carlo method (Carlson *et al.*, 2015; Chen and Zhang, 2017; Smith and Brown, 2020), the self-consistent Green's function method (Dickhoff and Barbieri, 2004), and Brueckner-Hartree-Fock (BHF) approaches (ter

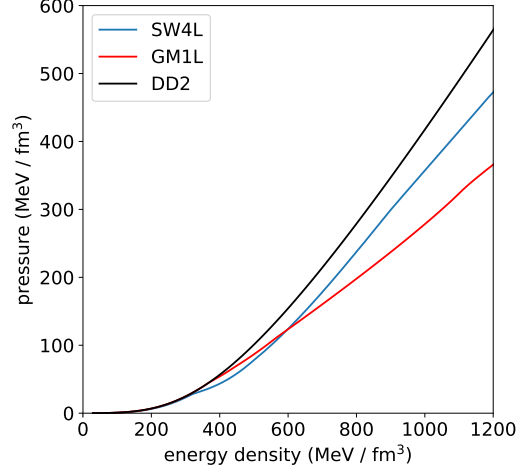


Fig. 1.1: Pressure as a function of energy density of neutron star matter for three nuclear parameter sets: SW4L (containing the ϕ and σ^* mesons), GM1L, and DD2.

Haar and Malfliet, 1986; Ter Haar and Malfliet, 1987; Poschenrieder and Weigel, 1988a,b; Brockmann and Machleidt, 1990; Sehn *et al.*, 1997; Gross-Boelting *et al.*, 1999; Van Dalen *et al.*, 2004; Tong *et al.*, 2018). For the context of this work, we will focus on the RMF approximation (Walecka, 1974; Boguta and Bodmer, 1977; Serot and Walecka, 1986; Reinhard, 1989) but a more complete explanation of the varying approximations can be found in Weber (1999); Glendenning (2012a); Spinella and Weber (2020).

In Fig. 1.1, we display the nuclear equations of state computed for three prominent RMF parametrization sets: DD2 (Typel *et al.*, 2010; Typel, 2018), SW4L (Spinella and Weber, 2019; Malfatti *et al.*, 2020), and GM1L (Spinella, 2017; Spinella *et al.*, 2018). The DD2 and GM1L models were recently employed in investigations by Malfatti *et al.* (2019) and Farrell *et al.* (2023), where the properties of hot neutron star matter and proto-neutron stars (Pons *et al.*, 1999) were studied. The Lagrangian is given by (refer also to Weber (1999); Glendenning (2012b); Spinella and Weber (2020); Sedrakian *et al.* (2022)):

$$\begin{aligned}
\mathcal{L} = & \sum_B \bar{\psi}_B [\gamma_\mu (i\partial^\mu - g_{\omega B}\omega^\mu - g_{\rho B}\boldsymbol{\tau} \cdot \boldsymbol{\rho}^\mu) - (m_B - g_{\sigma B}\sigma)] \psi_B \\
& + \frac{1}{2} (\partial_\mu \sigma \partial^\mu \sigma - m_\sigma^2 \sigma^2) - \frac{1}{3} \tilde{b}_\sigma m_N (g_{\sigma N} \sigma)^3 - \frac{1}{4} \tilde{c}_\sigma (g_{\sigma N} \sigma)^4 \\
& - \frac{1}{4} \omega_{\mu\nu} \omega^{\mu\nu} + \frac{1}{2} m_\omega^2 \omega_\mu \omega^\mu + \frac{1}{2} m_\rho^2 \boldsymbol{\rho}_\mu \cdot \boldsymbol{\rho}^\mu - \frac{1}{4} \boldsymbol{\rho}_{\mu\nu} \cdot \boldsymbol{\rho}^{\mu\nu},
\end{aligned} \tag{1.11}$$

where ψ_B represents the various baryon fields, $g_{\sigma B}$, $g_{\omega B}$, and $g_{\rho B}$ are (density-dependent) meson-baryon coupling constants, and \tilde{b}_σ and \tilde{c}_σ denote two additional coupling parameters associated with non-linear (cubic and quartic) self-interactions introduced by Boguta and Bodmer (1977). The SW4L models incorporate extra ϕ

Table 1.2: Properties of symmetric nuclear matter at saturation density for the SW4L, GM1L, and DD2 nuclear parametrizations.

Saturation property	Units	SW4L	GM1L	DD2
n_0	fm^{-3}	0.150	0.153	0.149
E_0	MeV	-16.0	-16.3	-16.02
K_0	MeV	250.0	300.0	242.7
m_N^*/m_N		0.70	0.70	0.56
J_0	MeV	30.3	32.5	32.8
L_0	MeV	46.5	55.0	55.3
U_N	MeV	-64.6	-65.5	-75.2

and σ^* mesons whose Lagrangians are given by [Spinella and Weber (2019)]

$$\mathcal{L}_\phi = -\frac{1}{4}\phi^{\mu\nu}\phi_{\mu\nu} + \frac{1}{2}m_\phi^2\phi_\mu\phi^\mu \quad (1.12)$$

and

$$\mathcal{L}_{\sigma^*} = \frac{1}{2}(\partial_\mu\sigma^*\partial^\mu\sigma^* - m_{\sigma^*}^2\sigma^*\sigma^*). \quad (1.13)$$

Note that the incorporation of ϕ and σ^* mesons also modifies the covariant derivative and the baryon B mass terms in the Lagrangian of Eq.1.12 by adding $-g_{\phi B}\phi^\mu$ and $-g_{\sigma^* B}\sigma^*$ in the respective parentheses. For all parametrizations, the leptons are described by

$$\mathcal{L}_l = \bar{\psi}_l(i\gamma_\mu\partial^\mu - m_l)\psi_l. \quad (1.14)$$

The saturation properties of symmetric nuclear matter for these models are shown in Table 1.2. These properties encompass nuclear saturation density n_0 , energy per nucleon E_0 , nuclear compressibility K_0 , effective nucleon mass m_N^*/m_N , asymmetry energy J_0 , asymmetry energy slope L_0 , and the value of the nucleon potential U_N . The values of L_0 listed in Table 1.2 are consistent with the value of the slope of the symmetry energy deduced from nuclear experiments and astrophysical observations (Oertel *et al.*, 2017).

The equations of state shown in Fig. 1.1 include all particles of the spin- $\frac{1}{2}$ baryon octet, comprising the nucleons (n, p) and hyperons ($\Lambda, \Sigma^+, \Sigma^0, \Sigma^-, \Xi^0, \Xi^-$). Additionally, all states of the spin- $\frac{3}{2}$ delta isobar $\Delta(1232)$ ($\Delta^{++}, \Delta^+, \Delta^0, \Delta^-$) are taken into account self-consistently. A detailed discussion of the choices for the meson-baryon coupling constants can be found in Malfatti *et al.* (2019, 2020) and in Spinella and Weber (2020).

Figures 1.2 through 1.5 showcase the relative particle fractions in dense neutron star matter at temperatures ranging from 1 MeV (representing cold matter) to 75 MeV. These compositions adhere to the constraints of electric charge neutrality and chemical equilibrium, which are maintained at every density. The delicate equilibrium between positively and negatively charged particles is crucial to ensuring the electric charge neutrality of the matter in the stellar core of a neutron star. Finite temperatures induce alterations in the particle composition within the neutron star core due to increased thermal energy. At higher temperatures, particles

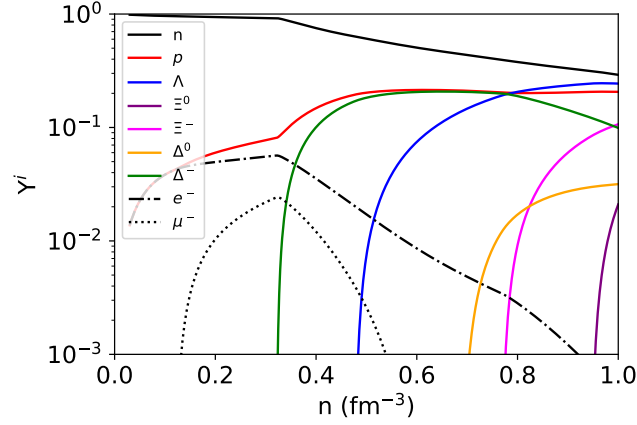


Fig. 1.2: Relative particle fractions Y^i ($= n_i/n$) in cold ($T=1$ MeV) neutron star matter determined with the SW4L model.

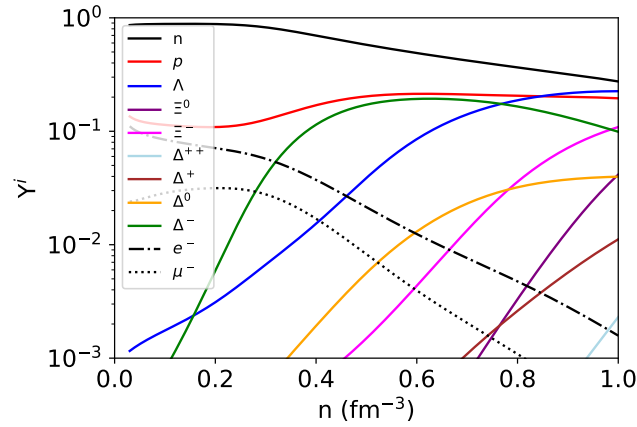


Fig. 1.3: Same as Fig. 1.2, but for neutron star matter at $T = 25$ MeV.

gain additional kinetic energy, leading to enhanced thermal motion. This process is governed by fundamental principles such as the Pauli exclusion principle, embodied in the Fermi-Dirac distribution, which dictates the occupation of fermions. The thermal population of states is critically influenced by these principles, impacting the equilibrium conditions that prevail at lower temperatures.

1.3.2 Strange Quark Stars and Strange Quark Matter

Quark stars are hypothetical compact objects in which matter would not be held together by gravitational attraction, but rather by the strong interaction between quarks. Notably, quark stars might possess a lower minimum mass and a smaller radius compared to neutron stars. Additionally, quark stars could feature an ex-

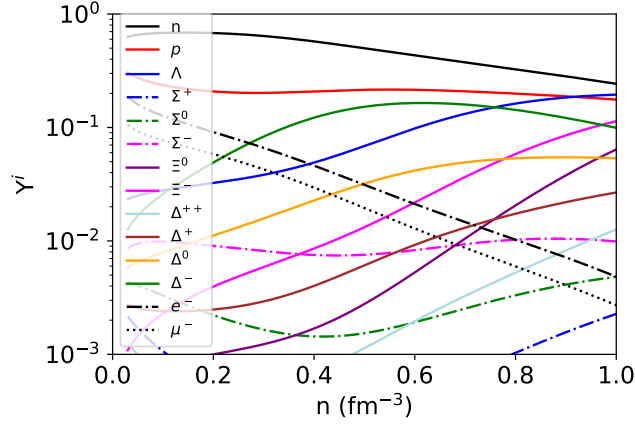


Fig. 1.4: Same as Fig. 1.2, but for neutron star matter at $T = 50$ MeV.

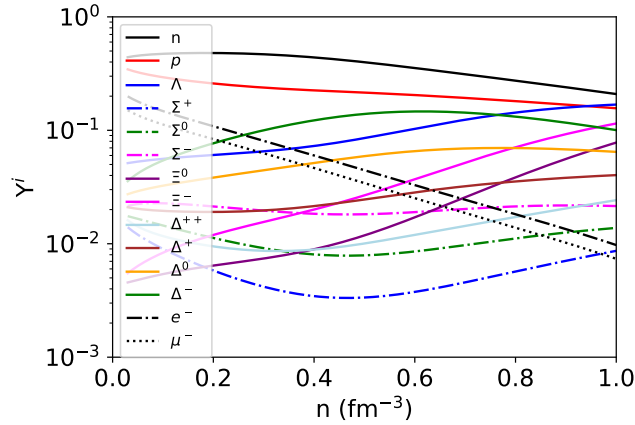


Fig. 1.5: Same as Fig. 1.2, but for neutron star matter at $T = 75$ MeV.

posed quark surface capable of emitting radiation at exceptionally high rates (Usov, 2001; Zakharov, 2011) or a thin crust of normal matter (Alcock *et al.*, 1986a; Glendenning and Weber, 1992; Glendenning *et al.*, 1995). The existence of quark stars has not been conclusively confirmed, but certain candidates, including RXJ1856.5-37544, PSR J1614-2230, 1E1207, SGR1806, and HESS J1731-347 have been proposed based on observational data [Xu (2003); Turolla *et al.* (2004); Weber (2005); Yuan *et al.* (2022); Kurban *et al.* (2022); Doroshenko *et al.* (2022); Horvath *et al.* (2023)].

The concept of quark stars was initially introduced in the 1970s and 1980s by several researchers (e.g., Itoh (1970b)) and gained prominence among theoretical astrophysicists, driven by the hypothesis that strange quark matter, composed of roughly equal numbers of u , d , and s quarks, could be more stable than the most stable atomic nucleus, which is ${}^{62}\text{Ni}$.

In 1971, Bodmer (Bodmer, 1971) introduced the concept of potentially collapsed atomic nuclei, a crucial element in the exploration of quark matter. The notion of collapsed atomic nuclei and the emergence of new states of matter with greater stability than conventional atomic nuclei were further articulated by Terazawa in 1979 (Terazawa, 1979) and by Witten in 1984 (Witten, 1984) who proposed that strange quark matter might exhibit greater stability than ^{56}Fe , the most stable element produced in astrophysical contexts, which is known as strange quark matter hypothesis. We note that it is a standard procedure to compare the energy of strange quark matter to ^{56}Fe . However, the energy per particle of ^{56}Fe ranks only third, following ^{62}Ni and ^{58}Fe .

Subsequent theoretical studies suggested that the ground state of deconfined quark matter could exist as a color superconductor with quarks forming diquarks similar to Cooper pairs in ordinary matter (Rajagopal and Wilczek, 2001; Alford, 2001; Alford *et al.*, 2008). One conceivable condensation pattern of color superconducting quark matter is the Color-Flavor-Locked (CFL) phase, yet numerous alternative condensation patterns have been proposed in the literature (Alford, 2001; Weber, 2005). If substantiated, this hypothesis could not only establish the reality of quark stars but also indicate their existence as color superconductors.

Building upon this hypothesis, the existence of strange white dwarfs was also proposed (Glendenning *et al.*, 1995). These would be compact objects distinct from traditional white dwarfs, forming either through the accumulation of normal nuclear matter on their surfaces or by incorporating strangelets found in the galaxy (Glendenning *et al.*, 1995).

Recently, the special case of the neutron star in the supernova remnant HESS J1731-37 has brought quark stars back into the spotlight (Doroshenko *et al.*, 2022). The estimated mass of this neutron star, $M < 0.8 M_{\odot}$, is much lower than that of any other known neutron star and, in fact, lower than what is believed to be necessary to form a neutron star. Therefore, the question arises of how such a light object could have formed and whether it is indeed a neutron star or a more exotic object that lost part of its mass in a transition from a neutron star to a quark star.

In this context, we dedicate part of this chapter to these exotic and hypothetical compact objects. Numerous studies investigating the properties of quark stars have been conducted over the past several decades, with a renewed interest in the topic following observations like HESS J1731-37 and the detection of gravitational waves from stellar binary mergers. Recently, the first fully general relativistic modeling of a merger of two quark stars was conducted [Zhu and Rezzolla (2021)], which discusses the dynamical mass lost [Zhu and Rezzolla (2021)] and the threshold mass for prompt collapse into a black hole for a quark star binary [Zhou *et al.* (2022)]. For a recent examination of the stability of rotating quark stars, we direct readers to the works of [Zhou *et al.* (2021); Chen and Lin (2023)] and the references contained therein.

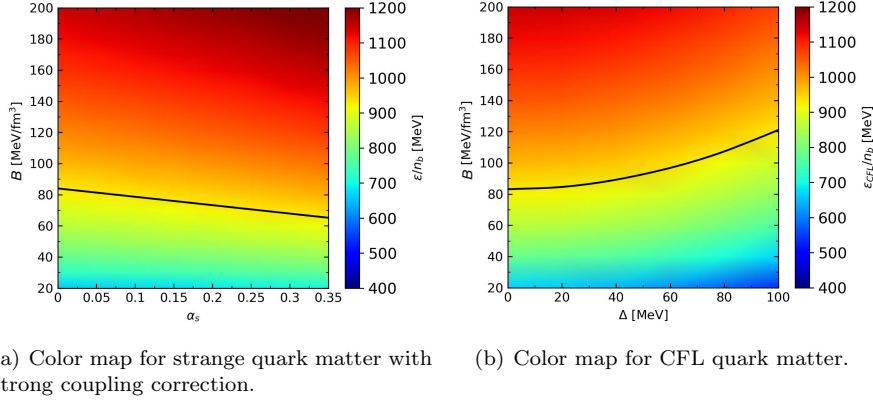


Fig. 1.6: Absolute stability of strange quark matter with respect to an ^{56}Fe nucleus. Energy per baryon is presented as a color map in the B - α_s plane, panel (a), (B - Δ plane, panel (b)), for strange (CFL) quark matter within the MIT Bag model (see text for details). The black curve represents the constraint corresponding to the ^{56}Fe mass. Only B - α_s and B - Δ pairs below the black curves result in combinations for EOS that lead to stable astrophysical configurations.

1.3.2.1 Equation of State of Quark Matter and Stability Windows

To construct self-bound quark stars, we will use two descriptions for the EOS of the matter that composes them: quark matter with corrections due to the strong coupling constant, and quark matter in color superconducting CFL state.

Corrections in bulk quark matter due to strong coupling constant, α_s , were included by [Farhi and Jaffe (1984)] in 1984. In the case where the quark gas interacts strongly, $O(\alpha_s)$ corrections (being α_s the strong coupling constant among quarks) must be made through the perturbative expansion of QCD, developing an improved renormalization group. To do this, a renormalization point ρ where $m(\rho)$ and $\alpha_s(\rho)$ are defined must be chosen. Specifically, $\rho = M_N/3 = 313$ MeV was chosen, where M_N is the mass of the neutron. Thus, the pressures for light quarks are as follows:

$$P_u = \frac{\mu_u^4}{4\pi^2} \left(1 - \frac{2\alpha_s}{\pi}\right), \quad (1.15)$$

$$P_d = \frac{\mu_d^4}{4\pi^2} \left(1 - \frac{2\alpha_s}{\pi}\right), \quad (1.16)$$

$$\begin{aligned}
P_s = \frac{1}{4\pi^2} \left\{ \mu_s (\mu_s^2 - m_s^2)^{1/2} (\mu_s^2 - \frac{5}{2} m_s^2) + \frac{3}{2} m_s^4 \ln \frac{\mu_s + (\mu_s^2 - m_s^2)^{1/2}}{m_s} \right. \\
\left. - \frac{2\alpha_s}{\pi} \left[3 \left(\mu_s (\mu_s^2 - m_s^2)^{1/2} - m_s^2 \ln \frac{\mu_s + (\mu_s^2 - m_s^2)^{1/2}}{\mu_s} \right)^2 \right. \right. \\
\left. \left. - 2(\mu_s^2 - m_s^2)^2 + 3m_s^4 \ln \left(\frac{m_s}{\mu_s} \right)^2 + 6 \ln \left(\frac{\rho}{\mu_s} \right) \left(\mu_s m_s^2 (\mu_s^2 - m_s^2)^{1/2} \right. \right. \right. \\
\left. \left. \left. - m_s^4 \ln \frac{\mu_s + (\mu_s^2 - m_s^2)^{1/2}}{m_s} \right) \right] \right\}, \quad (1.17)
\end{aligned}$$

where we have considered massless u and d quarks, the strange quark mass, $m_s = 96$ MeV; $\mu_i = \mu + q_i \mu_e$ is the chemical potential of the quark i , with electric charge q_i in β -equilibrium and μ_e is the chemical potential of the electron. The contribution of the electrons to the pressure is given by

$$P_e = \frac{\mu_e^4}{12\pi^2}. \quad (1.18)$$

For simplicity, muons are not included because their contribution to quark matter at zero temperature is negligible. The equation of state for quarks with corrections due to the strong coupling constant, within the MIT Bag model, arises from a mechanical-statistical or thermodynamic analysis in which the energy density is given by

$$\varepsilon = \sum_{i=u,d,s,e} (\mu_i n_i - P_i) + B, \quad (1.19)$$

where i ranges over the three quark flavors, and electron, arising from the condition of chemical equilibrium among the system's particles. The bag constant, B , acts as a vacuum energy per unit volume (or pressure) and takes into account the long-range interactions of QCD. The pressure due to the contribution of the three quarks in the CFL phase is given by (Smith *et al.*, 2009)

$$P_{\text{CFL}} = \frac{3\mu^4}{4\pi^2} (1 - c) - \frac{3\mu^2}{4\pi^2} (m_s^2 - 4\Delta^2) - B, \quad (1.20)$$

where $c = 2\alpha_s/\pi$ and Δ is the color superconducting gap, treated here as a free parameter. We will consider $c=0$ for the CFL phase. The energy density in this case is given by

$$\varepsilon_{\text{CFL}} = -P_{\text{CFL}} + \sum_{i=u,d,s} \mu_i n_i, \quad (1.21)$$

where $n_i = \partial P_{\text{CFL}} / \partial \mu_i$.

It is worth noting that matter in a CFL phase has properties similar to those of a superfluid (Alford *et al.*, 2008). In our phenomenological treatment of this phase, we have assumed electric and color charge neutrality. We have mentioned that quarks pair up to form Cooper pairs, implying that all quarks of different spins and flavors have the same Fermi momentum and, therefore, the same number density. This leads to the CFL phase being electrically neutral on average, allowing us to consider the presence of electrons negligible. While each Cooper pair contains one

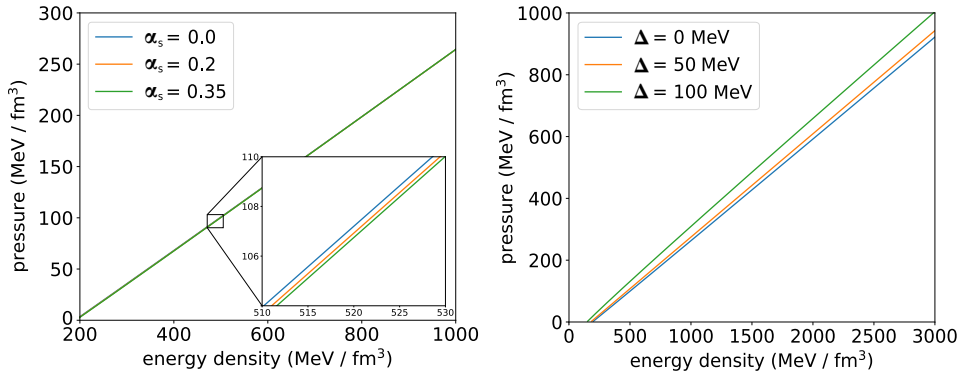


Fig. 1.7: Pressure as a function of energy density for quark matter modeled with the MIT Bag Model, where $B = 45 \text{ MeV}/\text{fm}^3$. The right panel demonstrates the impact of modifying the strong coupling constant α_s , while the left panel shows variations in the superconducting gap Δ within the Color-Flavor-Locked (CFL) phase. (See text for details).

quark of each of the three fundamental colors, we can also assume that the color combination in each Cooper pair is such that the total color charge of the CFL phase is zero.

As mentioned earlier, the hypothesis of absolute stability of quark matter suggests that this matter is the ground state of hadronic interactions, i.e., it is more stable than nuclear matter. In this definition, the critical pressure is zero: the true ground state of matter is always quark matter. Figure 1.6 shows the stability window of quark matter considered in this chapter. The black line in both figures corresponds to the mass of the most stable known element in nature that can be produced in astrophysical contexts, iron ^{56}Fe . Any combination of parameters below the black line in panels (a) and (b) of Fig. 1.6 gives us an appropriate equation of state for the construction of self-bound stars.

The EOS for the two models of quark matter considered in this chapter are shown in Figure 1.7. Increasing the strong coupling constant α_s or the superfluid gap Δ leads to a stiffened quark EOS: for the same energy density, the pressure is higher when these two parameters increase.

1.4 Properties of Strange Dwarfs

Continuing our exploration, we now direct our focus toward the unique characteristics of hypothetical strange dwarfs. These intriguing objects bear a resemblance to white dwarf stars but distinguish themselves by possessing cores composed of strange quark matter, which are enclosed within a conventional matter crust. Figure 1.8 illustrates the comprehensive mass-radius relationship of strange quark matter stars, encompassing a wide range from the compact members ('A') to the enigmatic strange dwarf objects ('C' to 'E'). The minimum masses of these sequences are confined within the rectangular area labeled 'B.' Notably, at 'D,' we find the

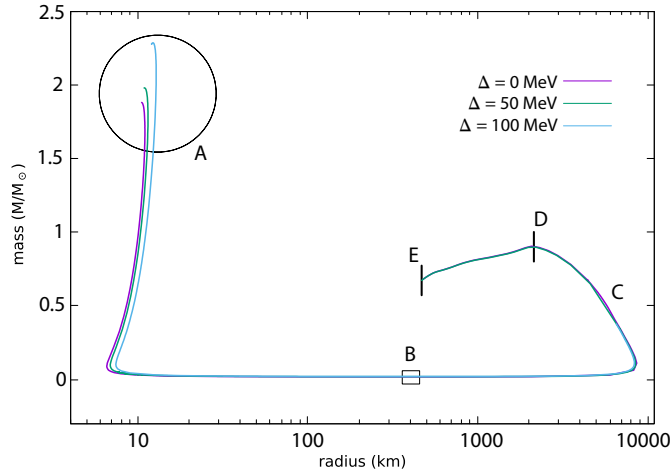


Fig. 1.8: Mass-radius relations for quark stars constructed with the MIT Bag Model varying the CFL superfluid gap Δ . The nuclear crust is described by the Baym-Pethick-Sutherland EOS. (See text for details.)

maximum-mass white dwarfs. However, it's essential to note that stars between 'D' and 'E' are prone to unstable radial oscillations. At point 'E,' the strange matter core at the center of white dwarfs has effectively shrunk to zero, resulting in the transformation into an ordinary white dwarf situated within the oscillatory unstable region.

The stability of strange dwarfs against radial perturbations was called into question by Alford and their collaborators in 2017, casting uncertainty on the potential existence of such celestial bodies (Alford *et al.*, 2017). Subsequent investigations by various research groups (Di Clemente *et al.*, 2023; Goncalves *et al.*, 2023) have shed light on this matter, demonstrating that strange dwarfs can indeed achieve stability under certain circumstances, provided that the transitions between quarks and hadrons occur at a slower rate than the radial perturbations themselves. Here, we proceed with the presumption that these conditions hold.

While it is not anticipated that strange matter endured the extreme conditions prevalent in the early Universe (Alcock and Farhi, 1985), there exist alternative scenarios for its generation. One such possibility is the formation of strange matter through the gravitational collapse of stellar cores during supernova explosions, with subsequent dissemination into the interstellar medium occurring during the merger of neutron stars with other compact objects (Bucciantini *et al.*, 2022). Despite these potential sources, strange stars and strange dwarfs have, thus far, eluded conclusive detection due to their striking resemblance to neutron stars and white dwarfs, respectively. Recently, reports have emerged suggesting possible candidates for strange dwarfs (Kurban *et al.*, 2022). Nevertheless, this situation may witness a transformative shift in the forthcoming years, chiefly owing to the advancements in gravitational wave astronomy. In particular, Perot *et al.* (Perot *et al.*, 2023), have demonstrated the feasibility of identifying hidden strange dwarfs within white

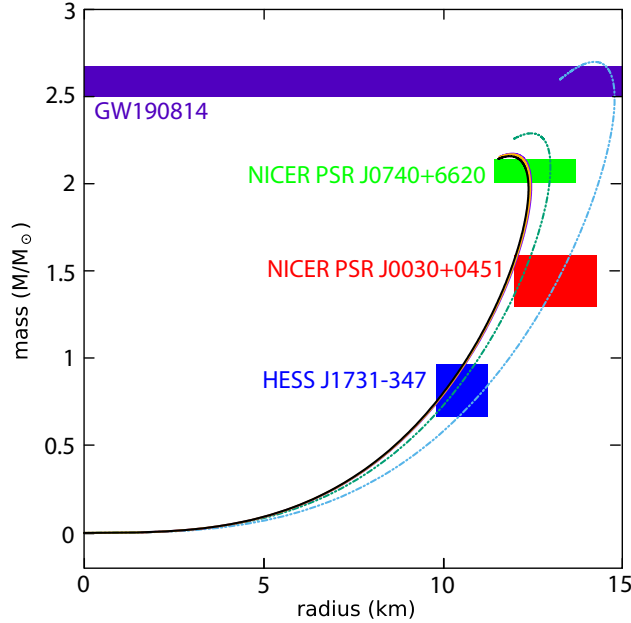


Fig. 1.9: Mass-radius relations for quark stars constructed within the MIT Bag Model, computed for different coupling constants α_s (shown with solid lines) and superfluid gaps Δ (shown with dashed lines), with $B = 45 \text{ MeV}/\text{fm}^3$, for the quark EOS models considered in this chapter. The results are compared with recent compact-star observations.

dwarf binary systems. This can be achieved through precise measurements of their tidal deformability utilizing future space-based gravitational-wave detectors, such as the Laser Interferometer Space Antenna (LISA). These groundbreaking developments hold the promise of unraveling the mysteries surrounding these novel celestial objects (Perot and Chamel, 2023).

1.5 Properties of Rotating Neutron Stars

Neutron stars can exhibit rigid body rotation, wherein the entire star rotates as a singular entity, maintaining a consistent rotation rate. Alternatively, neutron stars may display differential rotation, with different layers of the star rotating at varying rates. As neutron stars cool over time, diverse mechanisms come into play, leading to the damping of differential rotation and the establishment of uniform rotation. A crucial process in this transition is Eckman pumping, a phenomenon wherein the interaction between the star's magnetic field and its interior matter creates a torque that aligns the rotation axis of the star with its magnetic axis. This alignment process aids in reducing differential rotation by redistributing angular momentum within the star. The combination of angular momentum conservation during the collapse phase and subsequent processes like Eckman pumping guides

the evolution of neutron stars from initially hot and differentially rotating objects to cooler ones with more uniform rotation. Understanding these processes is essential for comprehending the internal dynamics, magnetic field evolution, and the overall lifecycle of neutron stars.

In this section, we provide a brief overview of the theoretical framework that elucidates the behavior of rotating neutron stars. We present results detailing the properties of neutron stars, focusing on both differentially rotating and uniformly rotating scenarios.

1.5.1 Uniform Rotation

To calculate neutron star properties, the stellar structure equations must be solved in the framework of Einstein's theory of general relativity. These equations are derived from Einstein's field equation and depend on the stellar matter's equation of state, or the underlying relationship between pressure P and energy density ϵ .

The simplest form of the stellar structure equations describes non-rotating, spherically symmetric objects in hydrostatic equilibrium. In this case, the stellar structure simplifies to an ordinary differential equation describing the pressure gradient within the star, known as the Tolman-Oppenheimer-Volkoff (TOV) equation (given in geometrical units where $G = c = 1$):

$$\frac{dP}{dr} = -\frac{(\epsilon + P)(m + 4\pi r^3 P)}{r^2 \left(1 - \frac{2m}{r}\right)}, \quad (1.22)$$

where m is the gravitational mass enclosed within a sphere of radius r , P is the pressure, and ϵ is the energy density. When integrating the TOV equation, one first would specify a value for the central density, ϵ_c , which in turn is used to determine the pressure value at the center of the star, P_c , using the specified EOS; at the center of the star ($r = 0$), the mass m and pressure differential P' disappear. For an infinitesimal increase in r , the mass of the star can be solved for as

$$\frac{dm}{dr} = 4\pi r^2 \epsilon. \quad (1.23)$$

The values ϵ_c , P_c , and m are used to solve for P' , thus allowing for the determination of P at the next radial step, which thus determines ϵ from the EOS. The computation of these parameters continues successively, increasing r until the pressure vanishes at the edge of the star. Then, the total gravitational mass M of a star can be deduced from the full radius R of the star as $M \equiv m(R) = 4\pi \int_0^R dr r^2 \epsilon$.

Rotating neutron star calculations are performed in the framework of general relativity and depend on the matter's nuclear equation of state. Modeling rotating neutron stars is more complicated than spherically symmetric, non-rotating stars for a few reasons: rotation deforms neutron stars, stabilizes them against collapse, and drags along the local inertial frames inside and outside of them so that they co-rotate with the stars (Mellinger Jr *et al.*, 2017; Weber, 1999). Rapid rotation can cause deformation where the star flattens at the pole and radially expands in the equatorial direction; this deformation results in the stellar structure equations not only being dependent on the radial coordinate r but also on the polar coordinate

θ . Rotation is a physical mechanism that stabilizes massive stars against collapse, resulting in rotating neutron stars being able to sustain up to 20% more mass than their non-rotating counterparts (Kalogera and Baym, 1996). The increased mass of rotating stars alters the geometry of spacetime by introducing a dependence on the star's rotational frequency to the line element and self-consistency condition to the stellar structure equations to account for the dragging of local inertial frames (Weber, 1999).

To solve for properties of rotating stars, we begin with the metric, which has the form

$$ds^2 = -e^{\gamma-\rho} dt^2 + e^{2\alpha}(dr^2 + r^2 d\theta) + e^{\gamma-\rho} r^2 \sin^2 \theta (d\phi - \omega dt)^2, \quad (1.24)$$

where γ , ρ , α , and ω are metric functions dependent on the radial coordinate r and polar angle θ , and ω describes frame dragging due to rotation. These functions also implicitly depend on the star's angular velocity Ω . The metric functions are computed from Einstein's field equation

$$R^{\kappa\sigma} - \frac{1}{2} R g^{\kappa\sigma} = 8\pi T^{\kappa\sigma}, \quad (1.25)$$

where $R^{\kappa\sigma}$ is the Ricci tensor, R is the curvature scalar, and $g^{\kappa\sigma}$ is the metric tensor. $T^{\kappa\sigma}$ is the energy momentum tensor given by

$$T^{\kappa\sigma} = (\epsilon + P) u^\kappa u^\sigma + g^{\kappa\sigma} P, \quad (1.26)$$

where ϵ and P are supplied by the equation of state. The partial differential equations for the metric functions γ , ρ , α , and ω , which follow from Eq. (1.25), are to be solved self-consistently for a given rotational stellar frequency (Paschalidis and Stergioulas, 2017). The absolute constraint on rapid rotation is defined by mass shedding, occurring at the Kepler frequency, Ω_K . However, this limit might not be reached due to instabilities driven by gravitational radiation-reaction-driven instabilities known as r and f -modes (Andersson and Kokkotas, 2001; Paschalidis and Stergioulas, 2017; Bratton *et al.*, 2022). Certain classes of instabilities may be associated with the emission of gravitational waves from neutron stars [Orsaria *et al.* (2019)].

The Kepler frequency is determined by the centrifugal force and gravity. In classical Newtonian mechanics, the Kepler frequency can be defined as

$$\Omega_K = \sqrt{\frac{MG}{R^3}}, \quad (1.27)$$

but this formula is drastically modified in general relativity. Following the metric function shown in Eq. (1.5.1), the general relativistic Kepler frequency is defined in terms of the metric functions as

$$\Omega_K = \frac{e^\rho}{r} V + \omega \quad (1.28)$$

where the quantity V denotes the equatorial velocity given by

$$V = \frac{\omega'}{(8 + \gamma' - \rho')} r e^{-\rho} + \sqrt{\frac{\gamma' + \rho'}{(8 + \gamma' - \rho')} + \left(\frac{\omega'}{(8 + \gamma' - \rho')} r e^{-\rho} \right)^2}. \quad (1.29)$$

Equations (1.28) and (1.29) are to be evaluated self-consistently at the star's equatorial radius.

Once a set of self-consistent solutions are found for the metric potentials, bulk properties of neutron stars like mass, radius, and Ω can be determined.

Table 1.3: Maximum gravitational mass with corresponding radius and central density of non-rotating and uniformly rotating neutron stars modeled with the DD2 parameter set.

Rotation	Mass [M_{\odot}]	Radius [km]	ϵ_c [MeV/fm ³]
Non-rotating (TOV)	2.316	11.589	1100
Uniform (Ω_K)	2.637	13.111	1060

1.5.1.1 Results for Uniformly Rotating Compact Objects

This section presents comprehensive insights into the bulk properties of uniformly rotating neutron stars and quark stars. The calculations for uniformly rotating neutron stars utilize the nuclear DD2 model, as detailed in Section 1.3.1. Figure 1.10 provides results for both a sequence of non-rotating stars, computed using the TOV equation, as expressed in Eq. (1.22), and a sequence of uniformly rotating stars at their mass-shedding limits ($\Omega = \Omega_K$).

In Figure 1.10, the left pane illustrates the mass-radius relationships for both non-rotating and uniformly rotating stars. Correspondingly, the right pane of Fig. 1.10 presents the gravitational mass as a function of central energy density, with each sequence's maximum mass denoted by a solid black dot. The mass peak values for both the non-rotating and uniformly rotating sequences derived from the DD2 model are provided in Table 1.3, along with their respective radii and central energy density values. Notably, uniform rotation at the Kepler limit enhances the mass peak for the DD2 model by around 14%.

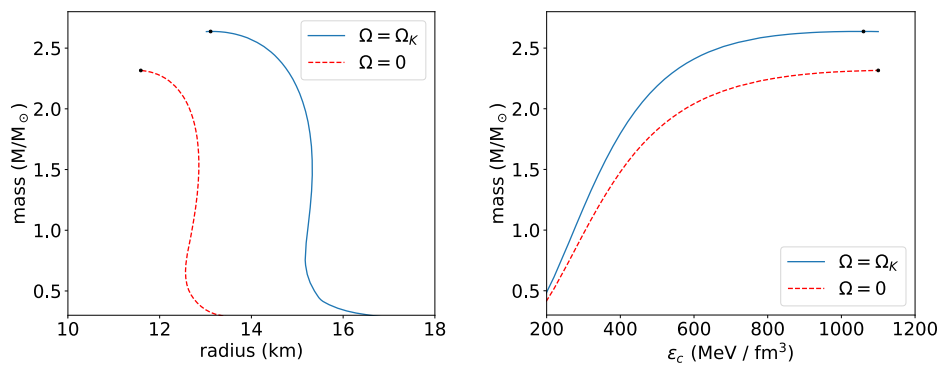


Fig. 1.10: Gravitational mass versus radius (left) and gravitational mass versus central stellar density (right) for both non-rotating ($\Omega = 0$) neutron stars and neutron stars rotating at the Kepler frequency ($\Omega = \Omega_K$), modeled with the DD2 nuclear EOS. Mass peaks are highlighted with black dots.

Table 1.4: Maximum gravitational mass with corresponding radius and central density of non-rotating and uniformly rotating quark stars for quark matter modeled within the MIT Bag Model with a bag constant $B = 45 \text{ MeV/fm}^3$.

Rotation	Max. Mass [M_{\odot}]	Radius [km]	ϵ_c [MeV/fm^3]
Non-rotating (TOV)	2.047	11.217	1100
Uniform (Ω_K)	2.413	13.250	900

To calculate the properties of uniformly rotating quark stars, the EOS for quark matter is modeled within the MIT Bag Model with a bag constant $B = 45 \text{ MeV/fm}^3$, as explained in Section 1.3.2.1. As for the DD2 model, a sequence of non-rotating stars and a sequence of uniformly rotating stars at their mass-shedding limit ($\Omega = \Omega_K$) for quark matter are shown in Figure 1.11.

The strange quark star sequences depicted in Fig. 1.11 are calculated for bare quark stars, consisting entirely of strange quark matter from the core to the surface. As discussed by Alcock *et al.* (1986a,b), strange quark stars however do not necessarily have to be bare; they can be surrounded by nuclear crusts, with densities at the crust's base lower than neutron drip density. Examples of strange stars with nuclear crusts are presented in Fig. 1.8. The thickness of the nuclear crust of the compact members of the stars shown there is typically just a few hundred meters or less (see Fig. 1.12) and the mass is below $\sim 10^{-5}M_{\odot}$ (Alcock *et al.*, 1986a). However, rapid rotation can moderately increase these values, as demonstrated by Glendenning and Weber (1992). The value of the mass peaks for both the non-rotating and uniformly rotating sequences for quark matter are given in units of M_{\odot} in Table 1.4 along with their corresponding radii and central energy density values. Uniform rotation at the Kepler limit for quark matter modeled within the MIT Bag Model increases the mass peak by 18% when compared to the non-rotating counterpart, a larger increase than that of the DD2 model.

The rotational period, P , of the uniformly rotating sequences from both the DD2 model and the MIT Bag Model can also be seen in Figure 1.13. At lower mass values, P is much higher for the nuclear EOS model DD2, but at their mass peaks, both the nuclear and quark EOS models see a similar value for P . In Figure 1.13, the horizontal black dotted line indicates the rotational period of the fastest observed MSP, PSR J1748–2446ad, with a rotational period of 1.3889 ms. The grey-shaded region schematically shows the period-mass range of all observed pulsars to date. The position of this region will shift downwards to shorter rotational periods if future pulsar discoveries unveil objects rotating below 1.3899 ms. Particularly, super-rapid rotation below approximately 1 ms, contingent on the mass, could suggest the presence of strange quark stars.

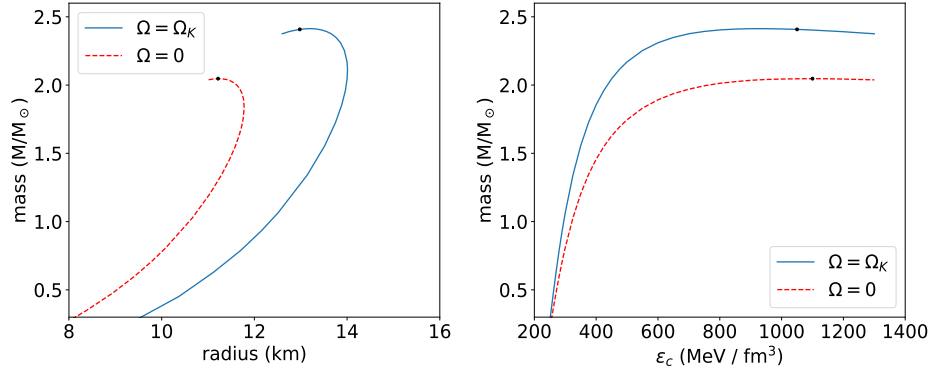


Fig. 1.11: Gravitational mass versus radius (left) and gravitational mass versus central density (right) of non-rotating ($\Omega = 0$) quark stars and quark stars rotating at the Kepler frequency ($\Omega = \Omega_K$), for quark matter modeled within the MIT Bag Model with $B = 45 \text{ MeV}/\text{fm}^3$. The mass peaks are indicated with black dots.

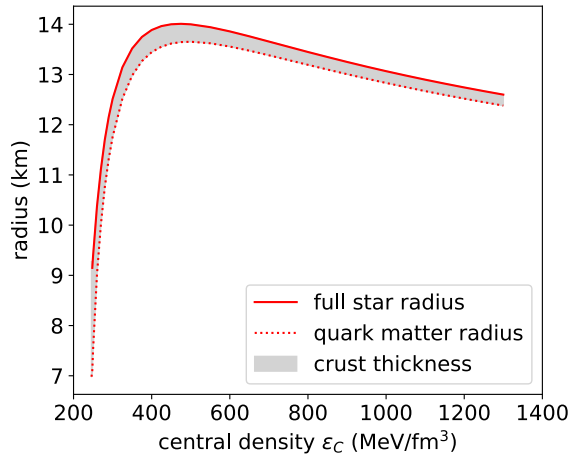


Fig. 1.12: The thickness of the nuclear crust of quark stars, with quark matter modeled using the MIT Bag Model, featuring a bag constant of $B = 45 \text{ MeV}/\text{fm}^3$.

1.5.2 Differential Rotation

While the majority of pulsars are believed to be rotating uniformly, some neutron stars form with an appreciable amount of differential rotation following extreme astrophysical events like core-collapse supernovae or binary neutron star mergers.

A newly formed proto-neutron star may experience some degree of differential rotation following a core-collapse supernova, but the phenomena would be short-lived. Hydrodynamical forces in the form of Ekman pumping and turbulent mixing will damp out any differential rotation in the star within a few days (Weber, 1999). A more likely avenue for a star to experience differential rotation is following a

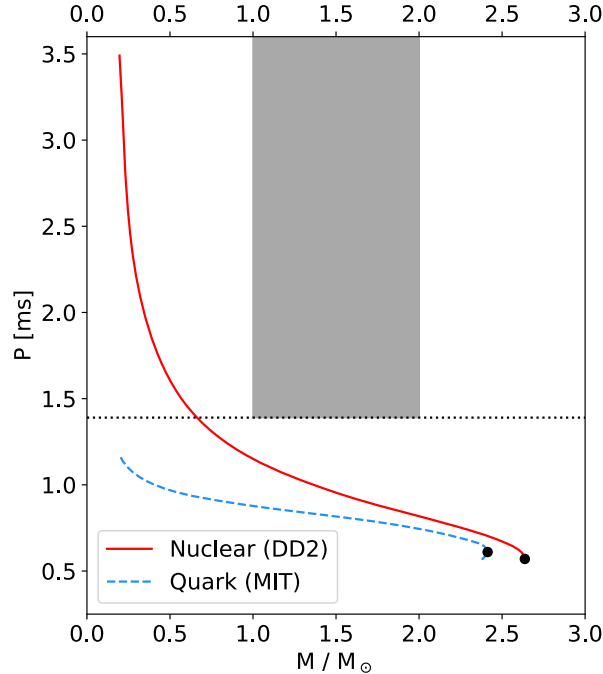


Fig. 1.13: Rotational periods P (in milliseconds) versus gravitational mass of both neutron stars and strange quark stars. Neutron stars are calculated using the DD2 nuclear EOS, while strange stars are modeled within the MIT Bag Model with the coupling constants $\alpha_s = 0$, the superfluid gap $\Delta = 0$ MeV, and a bag constant of $B = 45$ MeV/fm³. The black dotted line represents the period of the fastest observed MSP ($P = 1.3889$ ms), and the grey-shaded region denotes the range encompassing all observed pulsars to date.

binary neutron star merger event. When a neutron star binary coalesces, the two stars are most likely irrotational just prior to merging. The collision would result in a substantial velocity discontinuity at the surface of contact, giving rise to differentially rotating hypermassive or supramassive remnant stars. The remnant stars' fate depends largely on the dynamics and mass of the binary prior to merging. Many previous studies (Morrison *et al.*, 2004; Shapiro, 2000; Baumgarte *et al.*, 1999; Gondek-Rosińska *et al.*, 2017) have explored the implications of massive, differentially rotating neutron stars, but we extend this line of research to also include differentially rotating strange quark stars.

Differential rotation has physical implications that allow stars to remain stable in otherwise unstable configurations. Most notably, differentially rotating stars can support more mass than their uniformly rotating or non-rotating counterparts (Morrison *et al.*, 2004). In the case of massive remnant stars of binary merger events, differential rotation is one of the mechanisms that provide extra centrifugal

support to stabilize the star well above the TOV and uniform rotation mass limits.

The modeling of differential rotation begins with the same metric as uniform rotation. Once solved for, the metric functions are used to solve the equation of hydrostatic equilibrium for a barotropic fluid:

$$h(P) - h_p = \frac{1}{2}[\gamma_p + \rho_p - \gamma - \rho - \ln(1 - v^2) + F(\Omega)] \quad (1.30)$$

where $h(P)$ is the enthalpy as a function of pressure, and γ_p and ρ_p are the values of the metric potentials at the pole. The quantity v is defined as

$$v = (\Omega - \omega) r \sin \theta e^{-\rho}, \quad (1.31)$$

and the last term, $F(\Omega)$, defines the rotational law for the matter. Following the form in (Komatsu *et al.*, 1989; Cook *et al.*, 1992, 1994), the rotational law is set to

$$F(\Omega) = A^2(\Omega_c - \Omega), \quad (1.32)$$

where Ω_c is the central value for the angular velocity. In this equation, the parameter A is a constant scaling factor of the degree of differential rotation and is used to determine the length scale over which the frequency changes (Morrison *et al.*, 2004).

Simplifying Eq. (1.30) and including the rotation law gives

$$(\Omega_c - \Omega) = \frac{1}{A^2} \left[\frac{(\Omega - \omega) s^2 (1 - \mu^2) e^{-2\rho}}{(1 - s)^2 - (\Omega - \omega)^2 s^2 (1 - \mu^2) e^{-2\rho}} \right], \quad (1.33)$$

where the rotational frequency Ω can be isolated and solved numerically using a root-finding algorithm. The other non-defined parameters, s and μ , represent unitless radial and polar coordinates. Equation (1.5.2) uses a modified version of the rotation parameter, labeled \hat{A} , which is scaled by the equatorial radius r_e : $\hat{A} \equiv A/r_e$. Uniform rotation is achieved in the limit $\hat{A}^{-1} \rightarrow 0$, and has an upper bound of 1. The gravitational and matter fields are solved in a self-consistent fashion; once a set of self-consistent solutions to these equations is obtained, physical quantities like mass, radius, angular momentum, and rotational kinetic energy are outputted.

1.5.2.1 Results for Differentially Rotating Compact Objects

In this section, M-R relations for differentially rotating neutron stars and quark stars are shown. The M-R relations are calculated for different levels of differential rotation, varying the rotation parameter A in Eq. (1.32). Because the rotation parameter A repeatedly appears as \hat{A}^{-1} in the equations described in Section 1.5.2, we follow the lead of previous work which parameterized sequences by values of $\hat{A}^{-1} = 0.3, 0.5, 0.7,$ and 1.0 (Morrison *et al.*, 2004; Cook *et al.*, 1992; Galeazzi *et al.*, 2012). It's important to note that using the numerical scheme described in Section 1.5.2, the most extreme case of differential rotation ($\hat{A}^{-1} = 1.0$) may fail to find solutions at high central densities depending on the underlying EOS. In Fig. 1.14, the relationship between mass and central density ϵ_c is illustrated for the DD2 parameter set. This comparison involves three levels of differential rotation characterized by the rotation parameter \hat{A}^{-1} , contrasting them with the uniformly rotating (Kepler) and non-rotating (TOV) scenarios discussed in Section 1.5.1.1.

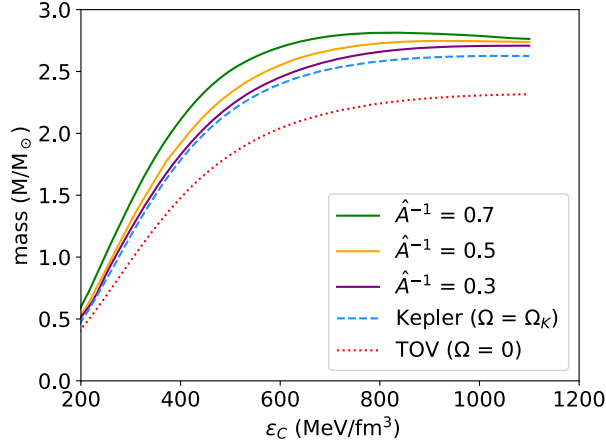


Fig. 1.14: Mass as a function of central density ϵ_c for the DD2 parameter set, comparing three degrees of differential rotation characterized by the rotation parameter \hat{A}^{-1} to the uniformly rotating (Kepler) and non-rotating (TOV) cases.

Table 1.5: Maximum gravitational mass with corresponding radius and central density of differentially rotating neutron stars, parametrized by three degrees \hat{A}^{-1} of differential rotation, modeled with the DD2 parameter set.

\hat{A}^{-1}	Mass [M_{\odot}]	Radius [km]	ϵ_c [MeV/fm ³]
0.3	2.66	13.05	1100
0.5	2.73	13.35	920
0.7	2.75	13.59	760

The figure underscores the influence of varying degrees of differential rotation on the mass-central density relationship. Table 1.5 provides detailed information on the maximum gravitational mass, corresponding radius, and central density for differentially rotating neutron stars. These models are parametrized by three levels of the rotation parameter \hat{A}^{-1} : 0.3, 0.5, and 0.7, as modeled with the DD2 parameter set. The results demonstrate how the introduction of differential rotation affects the stellar properties, with decreasing values of \hat{A}^{-1} gradually converging toward the uniform rotation scenario. This analysis highlights the nuanced impact of differential rotation on the stellar structure and provides a comprehensive understanding of the mass-central density relationship for neutron stars with varying degrees of rotation.

We next turn to investigating the impact of differential rotation on quark stars. Following the description in Section 1.3.2.1, six equation of state models are con-

Table 1.6: Maximum gravitational mass of quark stars (in units of M_{\odot}) for four degrees of differential rotation characterized by the rotation parameter \hat{A}^{-1} . The first three rows vary the strong coupling constant α_s , and the last three vary the superfluid gap Δ in the CFL phase.

Parametrization	$\hat{A}^{-1} = 0.3$	$\hat{A}^{-1} = 0.5$	$\hat{A}^{-1} = 0.7$	$\hat{A}^{-1} = 1.0$
$\alpha_s = 0.0$	2.384	2.476	2.579	2.664
$\alpha_s = 0.2$	2.391	2.443	2.546	2.597
$\alpha_s = 0.35$	2.353	2.411	2.506	2.549
$\Delta = 0$ MeV	2.379	2.492	2.576	2.651
$\Delta = 50$ MeV	2.525	2.647	2.732	2.767
$\Delta = 100$ MeV	2.917	3.037	3.162	3.193

structured: three models of quark matter with corrections due to the strong coupling constant, and three models of quark matter in the CFL phase. The three models with corrections due to the strong coupling constant, α_s , vary in the value of α_s (0.0, 0.2, and 0.35). The other three CFL models vary the parameter Δ , setting equal to 0, 50, or 100. For all six models, the bag constant B is set to $45 \text{ MeV}/\text{fm}^3$.

M-R relations for four different values of the rotation parameter \hat{A}^{-1} (0.3, 0.5, 0.7, and 1.0) are constructed for each EOS model. The M-R relations varying α_s are shown visually in Figure 1.15, and the M-R relations varying Δ are shown visually in Figure 1.16. The maximum gravitational mass from each curve for the four values of \hat{A}^{-1} are given in Table 1.6. The general trend for maximum mass expected when varying the value of \hat{A}^{-1} is to see higher mass values as $\hat{A}^{-1} \rightarrow 1.0$, which is reflected in Table 1.6. Additionally, stellar models with higher degrees of differential rotation struggle to find physical results at lower masses, as reflected in Figures 1.15 and 1.16 for both sets of quark matter EOS models.

The mass-radius relations in Figures 1.15 and 1.16 are constructed for a range of constant central densities ϵ_c . Two additional parameters are specified for each curve: the ratio of polar to equatorial ratio for the stellar models r_{ratio} and the given rotation parameter \hat{A}^{-1} . As the magnitude of differential rotation increases in a star, signified by $\hat{A}^{-1} \rightarrow 1$, the star grows more deformed, expanding at the equator, and thus decreases the r_{ratio} . For extremely high levels of differential rotation in massive stars, the star may even form the shape of a torus as $r_{\text{ratio}} \rightarrow 0$. The numerical scheme described in Section 1.5.2 uses the central density as the maximum density within the star which limits the lower threshold for the parameter r_{ratio} , so only quasi-toroidal configurations are possible for extreme differential rotation. The reader can find more information on modifying the specified numerical scheme to include fully toroidal configurations in Kaplan *et al.* (2014) and Morrison *et al.* (2004).

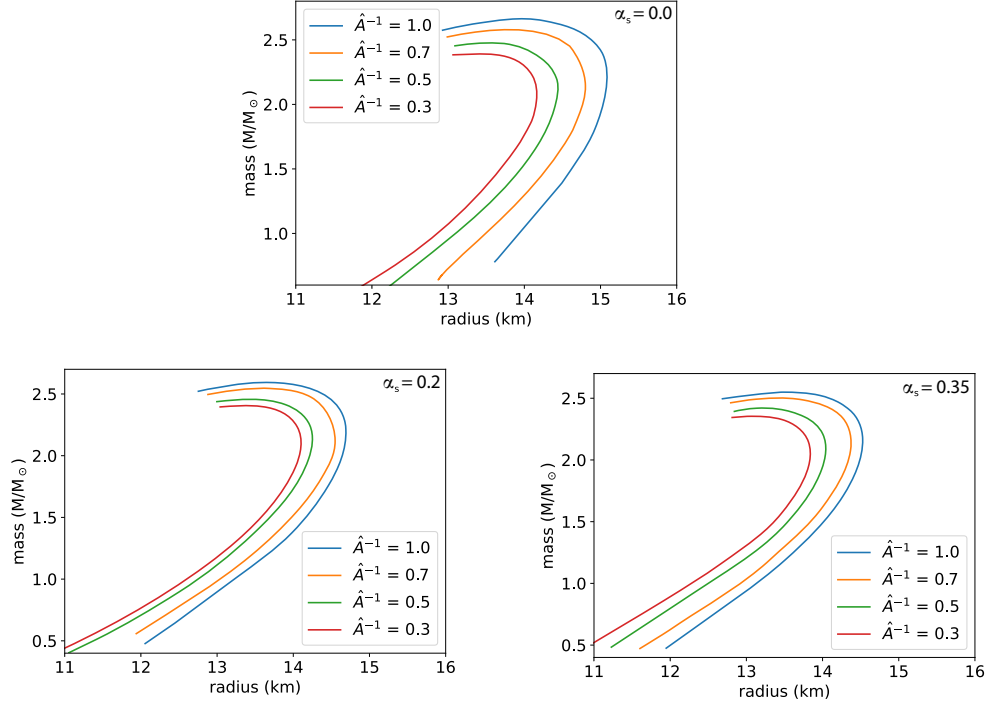


Fig. 1.15: Mass-radius relations of quark stars for the MIT Bag Model EOS with three values of the strong coupling constant α_s (0.0 on top, 0.2 on the bottom left, and 0.35 on the bottom right). Each figure depicts four degrees of differential rotation characterized by the scaled rotation parameter \hat{A}^{-1} .

1.6 Summary and Concluding Remarks

This chapter covers various topics related to neutron stars, addressing historical challenges in measuring their radius and the consequent uncertainties in size determination. Methods for radius estimation involve spectroscopic and timing techniques, with considerations for factors like magnetic fields and rapid rotation. Pulsar glitches or sudden spin jumps in neutron stars, provide insights into dense matter's EOS, revealing details about angular momentum transfer and interior dynamics. Tidal deformability, crucial in gravitational-wave astronomy, is explored in the context of binary neutron star mergers, with emphasis on the GW170817 event's contributions to mass, radius, and deformability estimates. The discussion extends to fast pulsars, categorizing them based on rotation, magnetic fields, and the role they play in astrophysical discoveries. The EOS of neutron stars is detailed, encompassing lower-density crust models and high-density core approaches. The chapter concludes by delving into quark stars, strange dwarfs, and the transformative possibilities of understanding these exotic objects through future observations and

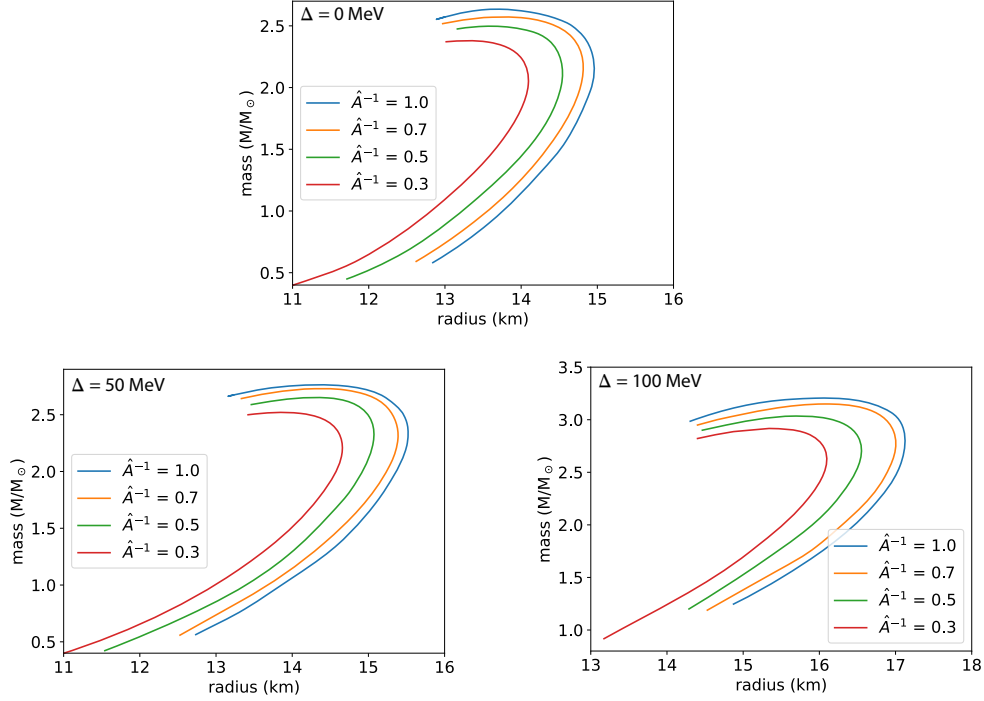


Fig. 1.16: Mass-radius relations of quark stars computed for the MIT Bag Model EOS with three values of Δ in the CFL phase (0 MeV on top, 50 MeV on the bottom left, and 100 MeV on the bottom right). Each figure depicts four degrees of differential rotation characterized by the scaled rotation parameter \hat{A}^{-1} .

gravitational wave detectors like LISA. Additionally, properties of rotating neutron stars are thoroughly examined, covering uniform and differential rotation scenarios, with insights into the impact of rotation on mass and radius, particularly after binary neutron star mergers. The comparison of maximum gravitational masses offers valuable information about the stability and deformations of rotating compact objects.

Key insights derived from the examination of fast pulsars, neutron stars, and astrophysical objects featuring strange quark matter include the following:

- (1) Historical challenges related to direct measurements of neutron star radius have resulted in uncertainties, necessitating the reliance on spectroscopic and timing techniques. Spectroscopic methods, particularly in low-mass X-ray binary systems, involve making assumptions about emitted spectra to infer mass-radius relations. However, challenges arise in cases of strong magnetic fields or rapid rotation.
- (2) Pulsar glitches offer a unique perspective into the equation of state of dense

neutron star matter, as the proposed models involve angular momentum transfer between the solid crust and the extremely dense interior, specifically the neutron superfluid.

- (3) Tidal deformability, crucial in gravitational-wave astronomy, is elaborated in the context of binary neutron star mergers. Theoretical calculations, along with the groundbreaking GW170817 event, contribute to estimates of masses, radii, and dimensionless tidal deformability.
- (4) Fast pulsars have played a pivotal role in testing theories of relativistic astrophysics. With over 3,000 observed pulsars to date, their numbers continue to grow rapidly with advancements in telescopes. Measuring pulsar rotation provides essential constraints on their bulk properties and the nature of the matter in their central cores. Superfast rotation, ideally with rotational periods below 1 millisecond, is expected to provide an additional observational window into the inner workings of neutron stars.
- (5) The equation of state (EOS), governing the pressure-density relationship within neutron stars, is crucial for understanding their internal structure. Models for the lower-density crust and high-density core are briefly discussed, emphasizing their role in simulations and observational analyses.
- (6) The intriguing concept of strange quark stars is explored. If they exist, such stars could be composed of quark matter in the color-flavor-locked phase, among other condensation patterns. The properties of strange dwarfs, characterized by conventional nuclear crusts and strange quark matter cores, are reviewed. Recently, potential implications for gravitational wave astronomy have been highlighted by Perot and Chamel (2023).

The discovery of stellar objects composed of absolutely stable strange quark matter remains an intriguing and challenging prospect in astrophysics. Detecting such objects presents a significant challenge due to the numerous observational signatures that overlap with those of ordinary neutron stars and white dwarfs. Distinguishing features may arise from ultra-rapid rotation (well below 1 ms), small radii (less than 10 km), and photon emission from the surface of a bare strange star. Proposed candidates, like the compact star RX J1856.5-3754, PSR J1614-2230, PSR J0348+0432, 4U 1820-30, and HESS J1731-347 have been considered, but definitive evidence is yet to be established. Advanced observational techniques and future space-based observatories, coupled with refined theoretical models, offer hope in the ongoing quest to unravel the mysteries of strange quark matter and identify potential stellar objects made of such matter.

- (7) Theoretical frameworks for calculating properties of rotating neutron stars are presented, covering uniform and differentially rotating scenarios. The impact of rotation on mass and radius is discussed using the DD2 model for the nuclear equation of state. Insights into stability and deformations are gained through comparisons of maximum gravitational masses.

Acknowledgments

This research was supported by the National Science Foundation (USA) under Grant No. PHY-2012152. MGO, IFR-S, and MC thank CONICET, UNLP and MinCyT (Argentina) for financial support under grants PIP-0169, 11/G187 and PICT 2019-3662. MC thanks Dr. Mauro Mariani and Marcos Celi for their assistance in creating the 3D figures for this chapter.

Bibliography

- Abbott, B. P., Abbott, R., Abbott, T. D., and et al. (2018). Gw170817: Measurements of neutron star radii and equation of state, *Phys. Rev. Lett.* **121**, p. 161101.
- Abbott, B. P. *et al.* (2017). Multi-messenger Observations of a Binary Neutron Star Merger, *ApJ* **848**, 2, L12.
- Abbott, R., Abbott, T., Abraham, S., Acernese, F., Ackley, K., Adams, A., Adams, C., Adhikari, R. X., Adya, V., Affeldt, C., *et al.* (2021). Constraints from ligo o3 data on gravitational-wave emission due to r-modes in the glitching pulsar psr j0537–6910, *The Astrophysical Journal* **922**, 1, p. 71.
- Agazie, G., Anumarlapudi, A., Archibald, A. M., Arzoumanian, Z., Baker, P. T., Bécsy, B., Blecha, L., Brazier, A., Brook, P. R., Burke-Spolaor, S., *et al.* (2023). The nanograv 15 yr data set: Evidence for a gravitational-wave background, *The Astrophysical Journal Letters* **951**, 1, p. L8.
- Alcock, C. and Farhi, E. (1985). Evaporation of strange matter in the early universe, *Phys. Rev. D* **32**, pp. 1273–1279.
- Alcock, C., Farhi, E., and Olinto, A. (1986a). Strange stars, *The Astrophysical Journal* **310**, pp. 261–272.
- Alcock, C., Farhi, E., Olinto, A., and Gleiser, M. (1986b). Quark stars and strange stars, *The Astrophysical Journal* **310**, pp. 772–778.
- Alcock, C. and Olinto, A. V. (1988). Ann. rev. nucl. part. sci. **38** (1988) 161, *Annual Review of Nuclear and Particle Science* **38**, p. 161.
- Alford, M. (2001). Ann. rev. nucl. part. sci. **51** (2001) 131, *Annual Review of Nuclear and Particle Science* **51**, p. 131.
- Alford, M. G., Harris, S. P., and Sachdeva, P. S. (2017). On the stability of strange dwarf hybrid stars, *The Astrophysical Journal* **847**, 2, p. 109.
- Alford, M. G., Schmitt, A., Rajagopal, K., and Schäfer, T. (2008). Color superconductivity in dense quark matter, *Reviews of Modern Physics* **80**, 4, pp. 1455–1515.
- Alpar, M., Langer, S. A., and Sauls, J. (1984). Rapid postglitch spin-up of the superfluid core in pulsars, *Astrophysical Journal, Part 1 (ISSN 0004-637X)*, vol. 282, July 15, 1984, p. 533–541. **282**, pp. 533–541.
- Ambartsumyan, V. A. and Saakyan, G. S. (1960). The Degenerate Superdense Gas of Elementary Particles, *Soviet Ast.* **4**, p. 187.
- Ambartsumyan, V. A. and Saakyan, G. S. (1961). On Equilibrium Configurations of Superdense Degenerate Gas Masses, *Astronom. Zhurnal* **38**, p. 785.
- Andersson, N. and Kokkotas, K. D. (2001). The r-mode instability in rotating neutron stars, *Int. J. Mod. Phys. D* **10**, pp. 381–441.
- ATLAS-Collaboration, G. A., Abat, E., Abdallah, J., Abdelalim, A. A., *et al.* (2008). The atlas experiment at the cern large hadron collider, *Journal of Instrumentation* **3**, 08, p. S08003.
- Basu, A., Shaw, B., Antonopoulou, D., Keith, M. J., Lyne, A. G., Mickaliger, M. B.,

- Stappers, B. W., Weltevrede, P., and Jordan, C. A. (2022). The jodrell bank glitch catalogue: 106 new rotational glitches in 70 pulsars, *Monthly Notices of the Royal Astronomical Society* **510**, 3, pp. 4049–4062.
- Baumgarte, T. W., Shapiro, S. L., and Shibata, M. (1999). On the maximum mass of differentially rotating neutron stars, *The Astrophysical Journal* **528**, 1, p. L29.
- Baym, G., Bethe, H. A., and Pethick, C. J. (1971a). Neutron star matter, *Nuclear Physics A* **175**, 2, pp. 225–271.
- Baym, G. and Chin, S. (1976). Phys. Lett. **62b** (1976) 241, *Physics Letters B* **62**, p. 241.
- Baym, G., Pethick, C., and Sutherland, P. (1971b). The ground state of matter at high densities: equation of state and stellar models, *The Astrophysical Journal* **170**, p. 299.
- Becker, W. (ed.) (2009). *Neutron Stars and Pulsars*, Astrophysics and Space Science Library (Springer, Berlin Heidelberg), ISBN 9783540769651.
- Bethe, H. A. and Johnson, M. B. (1974). Dense baryon matter calculations with realistic potentials, *Nucl. Phys. A* **230**, 1, pp. 1–58.
- Blaschke, D. and Chamel, N. (2018). *Phases of Dense Matter in Compact Stars*, chap. 7 (Springer International Publishing), ISBN 978-3-319-97616-7, pp. 337–400.
- Bodmer, A. R. (1971). Collapsed nuclei, *Phys. Rev. D* **4**, pp. 1601–1606.
- Boguta, J. and Bodmer, A. R. (1977). Relativistic calculation of nuclear matter and the nuclear surface, *NPA* **292**, p. 413.
- Bratton, E. L., Lin, Z., Weber, F., Orsaria, M. G., Ranea-Sandoval, I. F., and Saavedra, N. (2022). Gravitational-wave instabilities in rotating compact stars, *Galaxies* **10**, 5.
- Brockmann, R. and Machleidt, R. (1990). Relativistic nuclear structure. i. nuclear matter, *Physical Review C* **42**, 5, p. 1965.
- Brown, G. and Weise, W. (1976). Pion condensates, *Physics Reports* **27**, 1, pp. 1–34.
- Brown, G. E., Lee, C.-H., Rho, M., and Thorsson, V. (1994). From kaon-nuclear interactions to kaon condensation, *Nucl. Phys. A* **567**, 4, pp. 937–956.
- Bucciantini, N., Drago, A., Pagliara, G., Traversi, S., and Bauswein, A. (2022). Formation and evaporation of strangelets during the merger of two compact stars, *Phys. Rev. D* **106**, p. 103032.
- Burgio, G., Schulze, H.-J., Vidaña, I., and Wei, J.-B. (2021). Neutron stars and the nuclear equation of state, *Progress in Particle and Nuclear Physics* **120**, p. 103879.
- Carlson, J., Gandolfi, S., Pederiva, F., Pieper, S. C., Schiavilla, R., Schmidt, K., and Wiringa, R. B. (2015). Quantum monte carlo methods for nuclear physics, *Reviews of Modern Physics* **87**, 3, p. 1067.
- Chamel, N. and Haensel, P. (2008). Physics of neutron star crusts, *Living Reviews in Relativity* **11**, 1, p. 10.
- Chapline, G. and Nauenberg, M. (1977a). Ann. New York Academy of Sci. **302** (1977) 191, *Annals of the New York Academy of Sciences* **302**, p. 191.
- Chapline, G. and Nauenberg, M. (1977b). Phys. Rev. D **16** (1977) 450, *Physical Review D* **16**, p. 450.
- Chen, X. and Zhang, Y. (2017). Ab initio nuclear structure calculations with quantum monte carlo methods, *Journal of Computational Physics* **92**, 4, pp. 567–578.
- Collins, J. C. and Perry, M. J. (1975). Superdense matter: Neutrons or asymptotically free quarks? *Phys. Rev. Lett.* **34**, pp. 1353–1356.
- Cook, G. B., Shapiro, S. L., and Teukolsky, S. A. (1992). Spin-up of a rapidly rotating star by angular momentum loss-effects of general relativity, *The Astrophysical Journal* **398**, pp. 203–223.
- Cook, G. B., Shapiro, S. L., and Teukolsky, S. A. (1994). Rapidly rotating neutron stars in general relativity: Realistic equations of state, *The Astrophysical Journal* **424**, pp. 823–845.

- Cromartie, H. T., Fonseca, E., Ransom, S. M., Demorest, P. B., Arzoumanian, Z., Blumer, H., Brook, P. R., DeCesar, M. E., Dolch, T., Ellis, J. A., *et al.* (2020). Relativistic Shapiro delay measurements of an extremely massive millisecond pulsar, *Nature Astronomy* **4**, 1, pp. 72–76.
- De Luca, V., Franciolini, G., and Riotto, A. (2021). Nanograv data hints at primordial black holes as dark matter, *Physical Review Letters* **126**, 4, p. 041303.
- Di Clemente, F., Drago, A., Char, P., and Pagliara, G. (2023). Stability and instability of strange dwarfs, *A&A* **678**, p. L1.
- Dickhoff, W. and Barbieri, C. (2004). Self-consistent green’s function method for nuclei and nuclear matter, *Progress in Particle and Nuclear Physics* **52**, 2, pp. 377–496.
- Dietrich, T., Coughlin, M. W., Pang, P. T., Bulla, M., Heinzl, J., Issa, L., Tews, I., and Antier, S. (2020). Multimessenger constraints on the neutron-star equation of state and the Hubble constant, *Science* **370**, 6523, pp. 1450–1453.
- Doroshenko, V., Suleimanov, V., Pühlhofer, G., and Santangelo, A. (2022). A strangely light neutron star within a supernova remnant, *Nature Astronomy* **6**, 12, pp. 1444–1451.
- Farhi, E. and Jaffe, R. L. (1984). Strange matter, *Physical Review D* **30**, 11, pp. 2379–2390.
- Farrell, D., Alp, A., Weber, F., Spinella, W., Malfatti, G., Orsaria, M. G., and Ranea-Sandoval, I. F. (2023). *Hot Neutron Star Matter and Proto-neutron Stars*, chap. 5 (World Scientific), pp. 199–259.
- Fechner, W. B. and Joss, P. C. (1978). Nature **274** (1978) 347, *Nature* **274**, p. 347, doi: 10.1038/274347a0.
- Fritzsche, H., Gell-Mann, M., and Leutwyler, H. (1973). Advantages of the color octet gluon picture, *Physics Letters B* **47**, 4, pp. 365–368.
- Galeazzi, F., Yoshida, S., and Eriguchi, Y. (2012). Differentially-rotating neutron star models with a parametrized rotation profile, *Astronomy & Astrophysics* **541**, p. A156.
- Gendreau, K. C., Arzoumanian, Z., and *et al.* (2016). The neutron star interior composition explorer (nicer): Mission description, *The Astrophysical Journal* **832**, 2, p. 189.
- Glendenning, N. (2012a). *Compact Stars: Nuclear Physics*, *Particle Physics and General Relativity*, Astronomy and Astrophysics Library (Springer New York), ISBN 9781468404913.
- Glendenning, N. (2012b). *Compact Stars: Nuclear Physics, Particle Physics and General Relativity*, Astronomy and Astrophysics Library (Springer New York), ISBN 978-1-468-40491-3.
- Glendenning, N., Kettner, C., and Weber, F. (1995). Possible new class of dense white dwarfs, *Physical review letters* **74**, 18, p. 3519.
- Glendenning, N. K., Pei, S., and Weber, F. (1997). Signal of Quark Deconfinement in the Timing Structure of Pulsar Spin-Down, *Phys. Rev. Lett.* **79**, 9, pp. 1603–1606.
- Glendenning, N. K. and Schaffner-Bielich, J. (1999). First order kaon condensate, *Phys. Rev. C* **60**, 2, 025803.
- Glendenning, N. K. and Weber, F. (1992). Nuclear Solid Crust on Rotating Strange Quark Stars, *ApJ* **400**, p. 647.
- Goncalves, V. P., Jimenez, J. C., and Lazzari, L. (2023). Revisiting the stability of strange-dwarf stars and strange planets.
- Gondek-Rosińska, D., Kowalska, I., Villain, L., Ansorg, M., and Kucaba, M. (2017). A new view on the maximum mass of differentially rotating neutron stars, *The Astrophysical Journal* **837**, 1, p. 58.
- Gross-Boeltig, T., Fuchs, C., and Faessler, A. (1999). Covariant representations of the relativistic Brueckner t-matrix and the nuclear matter problem, *Nuclear Physics A* **648**, 1-2, pp. 105–137.
- Haensel, P., Potekhin, A. Y., and Yakovlev, D. G. (2007). *Neutron Stars 1* (Springer).

- Haensel, P. and Proszynski, M. (1982). Pion condensation in cold dense matter and neutron stars, *ApJ* **258**, pp. 306–320.
- Han, S. and Steiner, A. W. (2019). Tidal deformability with sharp phase transitions in binary neutron stars, *Phys. Rev. D* **99**, p. 083014.
- Harrison, B. K., Thorne, K. S., Wakano, M., and Wheeler, J. A. (1965). Gravitation theory and gravitational collapse, *Gravitation Theory and Gravitational Collapse*.
- Hessels, J. W., Ransom, S. M., Stairs, I. H., Freire, P. C., Kaspi, V. M., and Camilo, F. (2006). A radio pulsar spinning at 716 hz, *Science* **311**, 5769, pp. 1901–1904.
- Hewish, A., Bell, S. J., Pilkington, J. D., Frederick Scott, P., and Collins, R. A. (1979). Observation of a rapidly pulsating radio source, in *A Source Book in Astronomy and Astrophysics, 1900–1975* (Harvard University Press), pp. 498–504.
- Hinderer, T. (2008). Tidal love numbers of neutron stars, *The Astrophysical Journal* **677**, 2, p. 1216.
- Holder, J., Acciari, V. A., Aliu, E., and et al. (2006). The first veritas telescope, *Astroparticle Physics* **25**, 6, pp. 391–401.
- Horvath, J., Rocha, L., de Sá, L., Moraes, P., Barão, L., de Avellar, M., Bernardo, A., and Bacheaga, R. (2023). A light strange star in the remnant hess j1731- 347: Minimal consistency checks, *A&A* **672**, p. L11.
- Hughes, D. H., Briggs, F. H., Vogel, S. N., and et al. (2006). The green bank telescope, *The Astrophysical Journal* **131**, p. 450.
- Itoh, N. (1970a). Hydrostatic Equilibrium of Hypothetical Quark Stars, *Progress of Theoretical Physics* **44**, pp. 291–292.
- Itoh, N. (1970b). Hydrostatic Equilibrium of Hypothetical Quark Stars, *Progress of Theoretical Physics* **44**, 1, pp. 291–292.
- Ivanenko, D. D. and Kurdgelaidze, D. F. (1965). *Astrophys. J.* (1965) 251, *Astrophysics* **1**, p. 251.
- Jansen, F., Lumb, D., Altieri, B., and et al. (2001). Xmm-newton observatory. i. the spacecraft and operations, *Astronomy & Astrophysics* **365**, 1, p. L1.
- Jodrell Bank Observatory (Accessed: January 2022). Official website: Jodrell bank observatory.
- Johnston, S., Ball, L., Bonnardeau, M., and et al. (1996). The parkes multibeam pulsar survey, *Monthly Notices of the Royal Astronomical Society* **279**, pp. 1026–1046.
- Kalogera, V. and Baym, G. (1996). The maximum mass of a neutron star, *The Astrophysical Journal* **470**, 1, p. L61.
- Kaplan, D. B. and Nelson, A. E. (1988). Kaon condensation in dense matter, *Nucl. Phys. A* **479**, pp. 273–284.
- Kaplan, J., Ott, C., O’Connor, E., Kiuchi, K., Roberts, L., and Duez, M. (2014). The influence of thermal pressure on equilibrium models of hypermassive neutron star merger remnants, *The Astrophysical Journal* **790**, 1, p. 19.
- Kaspi, V. M. and Gavriil, F. P. (2017). Magnetars, *The Astrophysical Journal* **845**, 2, p. 148.
- Keister, B. D. and Kisslinger, L. S. (1976). *Phys. Lett.* **64b** (1976) 117, *Physics Letters B* **64**, p. 117.
- Knorren, R., Prakash, M., and Ellis, P. J. (1995). Strangeness in hadronic stellar matter, *Phys. Rev. C* **52**, 6, pp. 3470–3482.
- Komatsu, H., Eriguchi, Y., and Hachisu, I. (1989). Rapidly rotating general relativistic stars–i. numerical method and its application to uniformly rotating polytropes, *Monthly Notices of the Royal Astronomical Society* **237**, 2, pp. 355–379.
- Kurban, A., Huang, Y.-F., Geng, J.-J., and Zong, H.-S. (2022). Searching for strange quark matter objects among white dwarfs, *Physics Letters B* **832**, p. 137204.
- Lattimer, J. (2016). Observed neutron star masses.
- Lattimer, J. M. (2019). Neutron star mass and radius measurements, *Universe* **5**, 7.

- Lattimer, J. M. and Prakash, M. (2007). Neutron star observations: Prognosis for equation of state constraints, *Physics reports* **442**, 1-6, pp. 109–165.
- Lattimer, J. M. and Prakash, M. (2016). The physics of neutron stars, *Physics Reports* **621**, pp. 127–164.
- Lattimer, J. M. and Steiner, A. W. (2014). Constraints on the symmetry energy using the mass-radius relation of neutron stars, *The European Physical Journal A* **50**, 2, p. 40.
- Lee, C.-H., Jung, H., Min, D.-P., and Rho, M. (1994). Kaon-nucleon scattering from chiral Lagrangians, *Physics Letters B* **326**, 1-2, pp. 14–20.
- Leung, Y. C. and Wang, C. G. (1971). Properties of Hadron Matter. II. Dense Baryon Matter and Neutron Stars, *Ap. J.* **170**, p. 499.
- Link, B., Epstein, R. I., and Lattimer, J. M. (1999). Pulsar constraints on neutron star structure and equation of state, *Physical Review Letters* **83**, 17, p. 3362.
- Lorenz, C. P., Ravenhall, D. G., and Pethick, C. J. (1993). Neutron star crusts, *Phys. Rev. Lett.* **70**, pp. 379–382.
- Lorimer, D. and Ferrara, E. (2022). Galactic Millisecond Pulsars.
- Lorimer, D. R. (2008). Binary and millisecond pulsars, *Living reviews in relativity* **11**, 1, pp. 1–90.
- Machleidt, R. (1989). Advances in nuclear physics, *Advances in Nuclear Physics* **19**, p. 188.
- Machleidt, R., Holinde, K., and Elster, C. (1987). The nucleon-nucleon interaction, *Physics Reports* **149**, 1, p. 1.
- Madsen, J. (1999). Lecture notes in physics **516** (1999) 162, *Lecture Notes in Physics* **516**, p. 162.
- Madsen, J. (2007). Strange quark matter in astrophysics, *Advances in Space Research* **40**, 9, pp. 1389–1402.
- Makishima, K., Mihara, T., Nagase, F., and Tanaka, Y. (1999). Cyclotron resonance effects in two binary x-ray pulsars and the evolution of neutron star magnetic fields, *The Astrophysical Journal* **525**, 2, p. 978.
- Malfatti, G., Orsaria, M. G., Contrera, G. A., Weber, F., and Ranea-Sandoval, I. F. (2019). Hot quark matter and (proto-) neutron stars, *Phys. Rev. C* **100**, p. 015803.
- Malfatti, G., Orsaria, M. G., Ranea-Sandoval, I. F., Contrera, G. A., and Weber, F. (2020). Delta baryons and diquark formation in the cores of neutron stars, *Phys. Rev. D* **102**, p. 063008.
- Malik, T., Banik, S., and Bandyopadhyay, D. (2021). New equation of state involving Bose-Einstein condensate of antikaon for supernova and neutron star merger simulations, *European Physical Journal Special Topics* **230**, 2, pp. 561–566.
- Manchester, R. (2017). Millisecond pulsars, their evolution and applications, *Journal of Astrophysics and Astronomy* **38**, 3, p. 42.
- Mannarelli, M. (2019). Meson Condensation, *Particles* **2**, 3, pp. 411–443.
- Mellinger Jr, R. D., Weber, F., Spinella, W., Contrera, G. A., and Orsaria, M. G. (2017). Quark deconfinement in rotating neutron stars, *Universe* **3**, 1, p. 5.
- Melrose, D. (2017). Coherent emission mechanisms in astrophysical plasmas, *Reviews of Modern Plasma Physics* **1**, pp. 1–81.
- Migdal, A. B. (1972). Vacuum stability and limiting fields, *Soviet Physics Uspekhi* **14**, 6, pp. 813–813.
- Miller, M., Lamb, F. K., Dittmann, A., Bogdanov, S., Arzoumanian, Z., Gendreau, K. C., Guillot, S., Harding, A., Ho, W., Lattimer, J., *et al.* (2019). Psr j0030+ 0451 mass and radius from nicer data and implications for the properties of neutron star matter, *The Astrophysical Journal Letters* **887**, 1, p. L24.
- Miller, M. C., Lamb, F., Dittmann, A., Bogdanov, S., Arzoumanian, Z., Gendreau, K., Guillot, S., Ho, W., Lattimer, J., Loewenstein, M., *et al.* (2021). The radius of psr j0740+ 6620 from nicer and xmm-newton data, *The Astrophysical Journal Letters*

918, 2, p. L28.

- Miller, M. C. and Lamb, F. K. (2015). Determining neutron star properties by fitting oblate-star waveform models to x-ray burst oscillations, *The Astrophysical Journal* **808**, 1, p. 31.
- Morrison, I. A., Baumgarte, T. W., and Shapiro, S. L. (2004). Effect of differential rotation on the maximum mass of neutron stars: realistic nuclear equations of state, *The Astrophysical Journal* **610**, 2, p. 941.
- Moszkowski, S. A. (1974). Energy of neutron-star matter, *Phys. Rev. D* **9**, pp. 1613–1625.
- Nan, R., Li, D., Zhang, B., Fan, C., Qian, H., Cheng, J., Jin, Z., Lu, D., Li, X., Shao, Y., Jing, Z., Wu, X., Zhang, X., Cao, H., Yan, J., Yu, J., Wang, D., Wang, Q., Liu, D., Zheng, X., Yue, Y., Wang, G., Jiang, P., Zhang, K., Yang, J., Wang, Y., Yan, Y., Jin, Y., Jin, Y., Zhu, X., Fan, Y., Gao, Y., Dai, S., Han, Y., Zhang, H., Xu, Y., Wang, Y., Chen, Z., Zhang, S., You, X., Zhu, L., Qian, L., Wen, L., Jin, C., Zheng, W., Kong, L., Zhang, Y., Li, L., Qiu, K., Zhu, G., Xiao, L., Zhou, L., Gong, J., Lou, Y., Yang, S., Hu, K., Zhao, J., Chen, X., Wang, J., Zhang, Z., Deng, W., Zhang, K., Wang, J., Wang, H., Wang, J., Zhang, Z., Zhang, Z., Zhang, F., Xu, J., Li, H., Zhu, W., Yang, Y., Zhang, L., Lu, H., Zhang, X., Wang, X., Zhang, X., Yao, G., Lin, J., Li, J., Qi, Y., Zhang, Y., Yang, G., Zhu, M., Wu, X., Zhang, L., Chen, X., Cao, D., Cheng, J., Wang, Y., and Zheng, X. (2016). The five-hundred-meter aperture spherical radio telescope (fast) project, *International Journal of Modern Physics D* **25**, 08, p. 1641003.
- Negele, J. W. and Vautherin, D. (1973). Neutron star matter at sub-nuclear densities, *Nuclear Physics A* **207**, 2, pp. 298–320.
- Nelson, A. E. and Kaplan, D. B. (1987). Strange condensate realignment in relativistic heavy ion collisions, *Physics Letters B* **192**, 1-2, pp. 193–197.
- Oertel, M., Hempel, M., Klähn, T., and Typel, S. (2017). Equations of state for supernovae and compact stars, *Rev. Mod. Phys.* **89**, p. 015007.
- Orsaria, M. G., Malfatti, G., Mariani, M., Ranea-Sandoval, I. F., García, F., Spinella, W. M., Contrera, G. A., Lugones, G., and Weber, F. (2019). Phase transitions in neutron stars and their links to gravitational waves, *J. Phys. G: Nucl. Part. Phys.* **46**, 7, p. 073002.
- Özel, F. and Freire, P. (2016). Masses, radii, and the equation of state of neutron stars, *Annual Review of Astronomy and Astrophysics* **54**, pp. 401–440.
- Pandharipande, V. R. (1971). Hyperonic matter, *Nucl. Phys. A* **178**, pp. 123–144.
- Paschalidis, V. and Stergioulas, N. (2017). Rotating stars in relativity, *Living Reviews in Relativity* **20**, 1, p. 7.
- Perot, L. and Chamel, N. (2023). Role of quark matter and color superconductivity in the structure and tidal deformability of strange dwarfs, *Universe* **9**, 9.
- Perot, L., Chamel, N., and Vallet, P. (2023). Unmasking strange dwarfs with gravitational-wave observations, *Phys. Rev. D* **107**, p. 103004.
- Pethick, C., Ravenhall, D., and Lorenz, C. (1995). The inner boundary of a neutron-star crust, *Nuclear Physics A* **584**, 4, pp. 675–703.
- Pethick, C. J. and Ravenhall, D. G. (1999). The Physics of Neutron Star Crusts, in Z. Arzoumanian, F. Van der Hooft, and E. P. J. van den Heuvel (eds.), *Pulsar Timing, General Relativity and the Internal Structure of Neutron Stars*, p. 177.
- Piekarewicz, J., Fattoyev, F., and Horowitz, C. (2014). Pulsar glitches: The crust may be enough, *Physical Review C* **90**, 1, p. 015803.
- Pons, J. A., Reddy, S., Prakash, M., Lattimer, J. M., and Miralles, J. A. (1999). Evolution of Proto-Neutron Stars, *ApJ* **513**, pp. 780–804.
- Poschenrieder, P. and Weigel, M. (1988a). Nuclear matter problem in the relativistic green's function approach, *Physical Review C* **38**, 1, p. 471.
- Poschenrieder, P. and Weigel, M. (1988b). Nuclear matter properties in the relativistic

- λ -approximations, *Physics Letters B* **200**, 3, pp. 231–234.
- Predehl, P., Andriutschke, R., Becker, W., and et al. (2021). The erosita x-ray telescope on srg, *Astronomy & Astrophysics* **647**, p. A1.
- Rajagopal, K. and Wilczek, F. (2001). *The Condensed Matter Physics of QCD*, in M. Shifman (ed.), *At the Frontier of Particle Physics / Handbook of QCD* (World Scientific), p. 1.
- Rawley, L., Taylor, J., Davis, M., and Allan, D. (1987). Millisecond pulsar psr 1937+ 21: A highly stable clock, *Science* **238**, 4828, pp. 761–765.
- Reinhard, P.-G. (1989). Relativistic mean field theory - foundations and applications, *Reports on Progress in Physics* **52**, 4, pp. 439–513.
- Riley, T. E., Watts, A. L., Bogdanov, S., Ray, P. S., Ludlam, R. M., Guillot, S., Arzoumanian, Z., Baker, C. L., Bilous, A. V., Chakrabarty, D., et al. (2019). A nicer view of psr j0030+ 0451: millisecond pulsar parameter estimation, *The Astrophysical Journal Letters* **887**, 1, p. L21.
- Riley, T. E., Watts, A. L., Ray, P. S., Bogdanov, S., Guillot, S., Morsink, S. M., Bilous, A. V., Arzoumanian, Z., Choudhury, D., Deneva, J. S., et al. (2021). A nicer view of the massive pulsar psr j0740+ 6620 informed by radio timing and xmm-newton spectroscopy, *The Astrophysical Journal Letters* **918**, 2, p. L27.
- Rischke, D. H. (2004). Color superconductivity in cold dense quark matter, *Progress in Particle and Nuclear Physics* **52**, pp. 197–299.
- Rüster, S. B., Hempel, M., and Schaffner-Bielich, J. (2006). Outer crust of nonaccreting cold neutron stars, *Phys. Rev. C* **73**, p. 035804.
- Sammarruca, F. (2008). The” ab initio” approach to the nuclear equation of state: review and discussion, *arXiv preprint arXiv:0807.0263* .
- Sawyer, R. F. and Scalapino, D. J. (1973). Pion condensation in superdense nuclear matter, *Phys. Rev. D* **7**, pp. 953–964.
- Schaffner, J. and Mishustin, I. N. (1996). Hyperon-rich matter in neutron stars, *Phys. Rev. C* **53**, 3, pp. 1416–1429.
- Sedrakian, A. (2007). The physics of dense hadronic matter and compact stars, *Progress in Particle and Nuclear Physics* **58**, 1, pp. 168–246.
- Sedrakian, A., Li, J.-J., and Weber, F. (2022). *Hyperonization in Compact Stars* (WORLD SCIENTIFIC Publishing Company Incorporated), ISBN 978-9-811-22093-7.
- Sedrakian, A., Li, J. J., and Weber, F. (2023). Heavy baryons in compact stars, *Progress in Particle and Nuclear Physics* **475**, p. 104041.
- Sehn, L., Fuchs, C., and Faessler, A. (1997). Nucleon self-energy in the relativistic brueckner approach, *Physical Review C* **56**, 1, p. 216.
- Serot, B. D. and Walecka, J. D. (1986). Recent progress in quantum hadrodynamics, *Advances in Nuclear Physics* **16**, pp. 1–327.
- Shapiro, S. L. (2000). Differential rotation in neutron stars: Magnetic braking and viscous damping, *The Astrophysical Journal* **544**, 1, p. 397.
- Slane, P. O., Helfand, D. J., and Murray, S. S. (2002). New constraints on neutron star cooling from chandra observations of 3c 58, *The Astrophysical Journal* **571**, 1, p. L45.
- Smith, A. and Brown, D. (2020). Quantum monte carlo techniques in nuclear structure calculations, in R. Jones and S. White (eds.), *Advances in Nuclear Physics* (Springer), pp. 123–145.
- Smith, A. M., McFarquhar, G. M., Rauber, R. M., Grim, J. A., Timlin, M. S., Jewett, B. F., and Jorgensen, D. P. (2009). Microphysical and thermodynamic structure and evolution of the trailing stratiform regions of mesoscale convective systems during bamex. part i: Observations, *Monthly weather review* **137**, 4, pp. 1165–1185.
- Sotani, H., Yasutake, N., Maruyama, T., and Tatsumi, T. (2011). Signatures of hadron-quark mixed phase in gravitational waves, *Phys. Rev. D* **83**, p. 024014.

- Spinella, W. M. (2017). *A Systematic Investigation of Exotic Matter in Neutron Stars*, Ph.D. thesis, Claremont Graduate University & San Diego State University.
- Spinella, W. M. and Weber, F. (2019). Hyperonic neutron star matter in light of gw170817, *Astronomische Nachrichten* **340**, 1-3, pp. 145–150.
- Spinella, W. M. and Weber, F. (2020). *Dense Baryonic Matter in the Cores of Neutron Stars*, chap. 4 (World Scientific), pp. 85–152.
- Spinella, W. M., Weber, F., Orsaria, M. G., and Contrera, G. A. (2018). Neutrino Emissivity in the Quark-Hadron Mixed Phase, *Universe* **4**, 5, p. 64.
- Steiner, A. W., Heinke, C. O., Bogdanov, S., Li, C. K., Ho, W. C., Bahramian, A., and Han, S. (2018). Constraining the mass and radius of neutron stars in globular clusters, *Monthly Notices of the Royal Astronomical Society* **476**, 1, pp. 421–435.
- Stone, J. R. (2021). Nuclear physics and astrophysics constraints on the high density matter equation of state, *Universe* **7**, 8, p. 257.
- ter Haar, B. and Malfliet, R. (1986). Equation of state of nuclear matter in the relativistic dirac-brueckner approach, *Physical Review Letters* **56**, 12, p. 1237.
- Ter Haar, B. and Malfliet, R. (1987). Nucleons, mesons and deltas in nuclear matter a relativistic dirac-brueckner approach, *Physics Reports* **149**, 4, pp. 207–286.
- Terazawa, H. (1979). Dynamical subquark model of pregauged and pregeometric interactions, Tech. rep., Institute for Nuclear Study, University of Tokyo.
- Terazawa, H. (1991). Are super-hypernuclei found in cosmic rays? *Journal of the Physical Society of Japan* **60**, 6, pp. 1848–1851.
- Thapa, V. B., Sinha, M., Li, J. J., and Sedrakian, A. (2021). Massive Δ -resonance admixed hypernuclear stars with antikaon condensations, *Phys. Rev. D* **103**, p. 063004.
- Tong, H., Ren, X.-L., Ring, P., Shen, S.-H., Wang, S.-B., Meng, J., *et al.* (2018). Relativistic brueckner-hartree-fock theory in nuclear matter without the average momentum approximation, *Physical Review C* **98**, 5, p. 054302.
- Turolla, R., Zane, S., and Drake, J. J. (2004). Bare quark stars or naked neutron stars? the case of rx j1856. 5–3754, *The Astrophysical Journal* **603**, 1, p. 265.
- Typel, S. (2018). Relativistic Mean-Field Models with Different Parametrizations of Density Dependent Couplings, *Particles* **1**, 1, pp. 3–22.
- Typel, S., Röpke, G., Klähn, T., Blaschke, D., and Wolter, H. H. (2010). Composition and thermodynamics of nuclear matter with light clusters, *Phys. Rev. C* **81**, p. 015803.
- Usov, V. V. (2001). Thermal emission from bare quark matter surfaces of hot strange stars, *The Astrophysical Journal Letters* **550**, pp. L179 – L182.
- Van Dalen, E., Fuchs, C., and Faessler, A. (2004). The relativistic dirac-brueckner approach to asymmetric nuclear matter, *Nuclear Physics A* **744**, pp. 227–248.
- van Haarlem, M. P., Wise, M. W., Gunst, A. W., and *et al.* (2013). Lofar: The low-frequency array, *Astronomy & Astrophysics* **556**, p. A2.
- Walecka, J. D. (1974). A theory of highly condensed matter, *Annals of Physics* **83**, pp. 491–529.
- Watts, A. L., Andersson, N., Chakrabarty, D., Feroci, M., Hebeler, K., Israel, G., Lamb, F. K., Miller, M. C., Morsink, S., Özel, F., Patruno, A., Poutanen, J., Psaltis, D., Schwenk, A., Steiner, A. W., Stella, L., Tolos, L., and van der Klis, M. (2016). Colloquium: Measuring the neutron star equation of state using x-ray timing, *Rev. Mod. Phys.* **88**, p. 021001.
- Weber, F. (1999). *Pulsars as Astrophysical Laboratories for Nuclear and Particle Physics (Series in High Energy Physics, Cosmology and Gravitation)* (CRC Press), ISBN 0750303328.
- Weber, F. (2005). Strange quark matter and compact stars, *Progress in Particle and Nuclear Physics* **54**, 1, pp. 193–288.
- Weisskopf, M. C., O’Dell, S. L., van Speybroeck, L. P., and *et al.* (2000). The chandra x-ray observatory, *The Astrophysical Journal* **536**, 2, p. L81.

Bibliography

47

- Witten, E. (1984). Cosmic separation of phases, *Phys. Rev. D* **30**, pp. 272–285.
- Xu, R. X. (2003). Strange Quark Stars - A Review, in X. D. Li, V. Trimble, and Z. R. Wang (eds.), *High Energy Processes and Phenomena in Astrophysics*, Vol. 214 (Astronomical Society of the Pacific), p. 191.
- Yuan, W.-L., Li, A., Miao, Z., Zuo, B., and Bai, Z. (2022). Interacting ud and uds quark matter at finite densities and quark stars, *Phys. Rev. D* **105**, p. 123004.
- Zakharov, B. G. (2011). Photon emission from bare quark stars, *Journal of Experimental and Theoretical Physics* **112**, 1, pp. 63–76.
- Zhou, E., Kiuchi, K., Shibata, M., Tsokaros, A., and Uryū, K. b. o. (2021). Evolution of bare quark stars in full general relativity: Single star case, *Phys. Rev. D* **103**, p. 123011.
- Zhou, E., Kiuchi, K., Shibata, M., Tsokaros, A., and Uryū, K. 2022, Physical Review D, 106, 103030.
- Zhu, Z. and Rezzolla, L. 2021, Physical Review D, 104, 083004.
- Chen, K. and Lin, L.-M. 2023, Physical Review D, 108, 064007.